

Review

Microbubbles Stabilized by Protein Shell: From Pioneering Ultrasound Contrast Agents to Advanced Theranostic Systems

Polina G. Rudakovskaya ^{1,*}, Roman A. Barmin ^{1,†}, Pavel S. Kuzmin ², Elena P. Fedotkina ³ , Alexander N. Sencha ³ and Dmitry A. Gorin ^{1,*}

¹ Center for Photonic Science and Engineering, Skolkovo Institute of Science and Technology, Nobel Str. 3, 121205 Moscow, Russia; roman.barmin@skoltech.ru

² Institute of Materials for Modern Energy and Nanotechnology, Dmitry Mendeleev University of Chemical Technology of Russia, Miusskaya Sq. 9, 125047 Moscow, Russia; pavelkuzbmin@gmail.com

³ Research Center for Obstetrics, Gynecology and Perinatology, Ministry of Healthcare of the Russian Federation, Akademika Oparina Str. 4, 117198 Moscow, Russia; epf@yandex.ru (E.P.F.); asencha@yandex.ru (A.N.S.)

* Correspondence: p.rudakovskaya@skoltech.ru (P.G.R.); d.gorin@skoltech.ru (D.A.G.)

† These authors contributed equally to this work.

Abstract: Ultrasound is a widely-used imaging modality in clinics as a low-cost, non-invasive, non-radiative procedure allowing therapists faster decision-making. Microbubbles have been used as ultrasound contrast agents for decades, while recent attention has been attracted to consider them as stimuli-responsive drug delivery systems. Pioneering microbubbles were Albunex with a protein shell composed of human serum albumin, which entered clinical practice in 1993. However, current research expanded the set of proteins for a microbubble shell beyond albumin and applications of protein microbubbles beyond ultrasound imaging. Hence, this review summarizes all-known protein microbubbles over decades with a critical evaluation of formulations and applications to optimize the safety (low toxicity and high biocompatibility) as well as imaging efficiency. We provide a comprehensive overview of (1) proteins involved in microbubble formulation, (2) peculiarities of preparation of protein stabilized microbubbles with consideration of large-scale production, (3) key chemical factors of stabilization and functionalization of protein-shelled microbubbles, and (4) biomedical applications beyond ultrasound imaging (multimodal imaging, drug/gene delivery with attention to anticancer treatment, antibacterial activity, biosensing). Presented critical evaluation of the current state-of-the-art for protein microbubbles should focus the field on relevant strategies in microbubble formulation and application for short-term clinical translation. Thus, a protein bubble-based platform is very perspective for theranostic application in clinics.

Keywords: ultrasound; microbubbles; contrast agents; proteins; albumin; lysozyme; oleosin; drug delivery; theranostics



Citation: Rudakovskaya, P.G.; Barmin, R.A.; Kuzmin, P.S.; Fedotkina, E.P.; Sencha, A.N.; Gorin, D.A. Microbubbles Stabilized by Protein Shell: From Pioneering Ultrasound Contrast Agents to Advanced Theranostic Systems. *Pharmaceutics* **2022**, *14*, 1236. <https://doi.org/10.3390/pharmaceutics14061236>

Academic Editor: Yu-Fen Huang

Received: 25 April 2022

Accepted: 13 May 2022

Published: 10 June 2022

Publisher's Note: MDPI stays neutral with regard to jurisdictional claims in published maps and institutional affiliations.



Copyright: © 2022 by the authors. Licensee MDPI, Basel, Switzerland. This article is an open access article distributed under the terms and conditions of the Creative Commons Attribution (CC BY) license (<https://creativecommons.org/licenses/by/4.0/>).

1. Introduction

Ultrasound (US) imaging is a workhorse in clinical diagnostics routine, as it is non-invasive, low-cost, and requires no ionizing radiation [1,2]. US outperforms the number of magnetic resonance imaging (MRI) and computed tomography (CT) examinations by 2–3 times [3–5]. US relies on the piezoelectric effect when a device stimulated by an electric current emits and transmits ultrasound pulses and receives reflected echoes from organs and tissues to construct the image [6]. Poor contrast image quality can limit US usability for pathology diagnosis applications, such as hypervascular malignancies, or breast, liver, and renal masses [7,8]. The administration of contrast agents, initially demonstrated by Gramiak and Shah in 1968, can provide echogenicity several orders of magnitude higher than solid particles of comparable size [9–12]. Over the years, gas-filled microbubbles (MBs) have become the most popular US contrast agents with the ability to behave as a non-linear

oscillator and increase the detected signal intensity up to 1000 times. A brief timeline of the development of US imaging with contrast agents together with the development of albumin-based formulations is presented in Figure 1a.

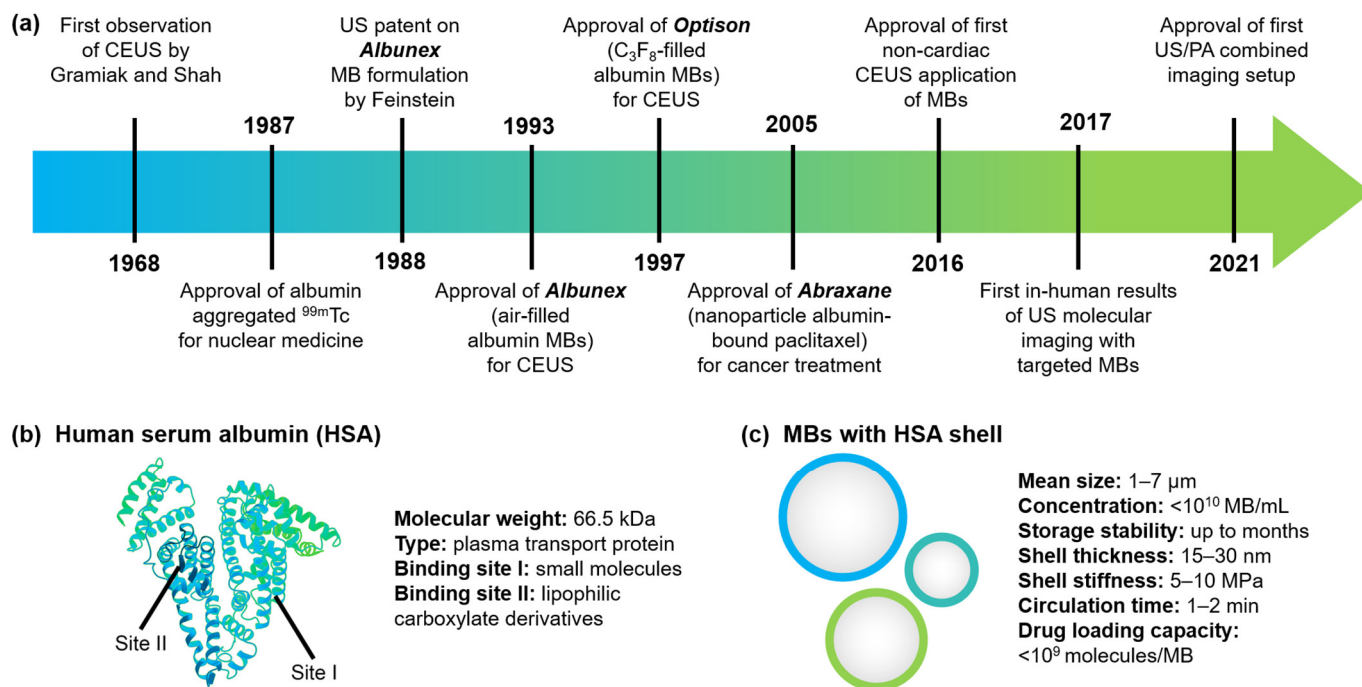


Figure 1. Microbubbles with albumin shell for ultrasound imaging. (a) Timeline of key advances in the field of ultrasound (US) contrast agents and albumin-based formulations development; key characteristics of (b) human serum albumin (HSA) and (c) microbubbles with an HSA shell. Abbreviations: US, ultrasound; CEUS, contrast-enhanced ultrasound; MBs, microbubbles; PA, photoacoustic; HSA, human serum albumin.

MBs are colloidal systems with a mean diameter of 1–7 μm , acting as real blood pool agents. Beyond imaging applications, MBs are actively investigated as drug delivery systems due to their shell drug loading capacities and gaseous core US stimuli-responsiveness [10,13–16]. An MB shell is mainly stabilized with lipids, proteins, or polymers [17–24]. Shell composition primarily affects MB performance regarding storage stability, circulation time, and stimuli response [25–29]. While lipid-based soft shell MBs are preferred for US imaging due to their optimal MB oscillation and resulting contrast profile; still, the gas can intensively diffuse, shortening MB stability. In contrast, polymeric hard shell MBs are preferred for drug delivery as their thicker shell can be loaded with higher amounts of drug molecules and prolongs MB stability, while a thicker shell can reduce contrast [13,17,22].

Protein MBs are a compromise solution with moderate properties between the soft lipid MB oscillation profile and the hard polymer MB drug loading capabilities [22,30–33]. Albumin is one of the most prominent proteins for pharmaceuticals [34–36]. The most abundant circulating protein in plasma, albumin serves as a versatile carrier for drug delivery and prolongs the active profile of fast-clearance drugs (Figure 1b). “Heart-shaped” protein, human serum albumin (HSA), provides two binding sites as pockets for small molecules, preferably aromatic dyes (by binding site 1) and lipophilic carboxylate derivatives (by binding site 2) [37–40]. In the past two decades, several HSA-based formulations have been approved by the Food and Drug Administration (FDA) for treatment [34,41].

Pioneering works of MB shell stabilization with albumin by Feinstein and Keller led to the regulatory approval of Albunex (Molecular Biosystems Inc., San Diego, CA, USA) in the USA in 1993 [42–44]. Albunex became the first commercially available left-heart US

contrast agent in the country with the formulation of sonicated human albumin and air [44]. Such an agent has revolutionized diagnostic US potential; however, MBs were pressure-sensitive, providing only a short-left ventricle contrast duration. Improved formulation of Albunex with a perfluorocarbons (C_3F_8) gas core instead of air demonstrated prolonged stability, reached approval in the USA in 1997 and is available as Optison (GE Healthcare AS, Oslo, Norway) [45–49]. Optison became the first US contrast agent using a gas other than air, opening the room for the approval of MBs loaded with perfluorocarbons as lipid-shelled Sonazoid (GE Healthcare AS, Oslo, Norway) and SonoVue (Bracco Suisse SA, Geneva, Switzerland) [50–52]. Recent works explore albumin-shelled MBs as drug delivery devices, exploring their applications beyond US imaging and aiming for short-term translation [20,53–55]. Key characteristics of HAS-shelled MBs are presented in Figure 1c.

Nowadays, ultrasound expands applications beyond imaging, especially with the MB introduction (Figure 1a). In 2016, MBs gained the US Food and Drug Administration approval for non-cardiac contrast [56]. First-in-human results of US molecular imaging with targeted agents were demonstrated in 2017 [57,58]. Targeted agent formulations entered clinical trials for tumor detection and liver lesion characterization [56,59]. In 2021, the combined ultrasound/photoacoustic imaging setup, the Imagio Breast Imaging System (Seno Medical Instruments, Inc., San Antonio, TX, USA), was approved for commercialization by the FDA, raising the question of smart multimodal/multifunctional agents development for advanced imaging [60,61]. Thus, therapeutic-aimed protein MBs act as an optimal candidate for short-term translation [20].

To boost the development of MBs with a protein shell for theranostics, it is crucial to summarize all efforts within the past two decades on (1) formulation of protein MBs, (2) advanced functionalization of the protein shell, and (3) application-driven implementation in biomedicine. Therefore, this review aims to summarize and critically evaluate known examples of protein MBs to enhance their applications in clinical practice.

2. Proteins Involved in MB Shell Stabilization

MB formation is enabled by lowering the surface tension of solutions at the gas-liquid interface with the introduction of surfactants [18,62–64]. Hence, various surfactants are used as the basis for MB fabrication. One of the optimal MB shell components is proteins [65,66]. Proteins are biocompatible polymers; natural proteins contain all-natural amino acids. Their presence provides protein amphiphilicity and a wide range of established functionalization routes. An important and insufficiently disclosed area at the moment is synthetic biopolymers based on oligopeptides for MB fabrication. At the moment, the main natural proteins used for MB fabrication are (Figure 2): bovine and human serum albumins (BSA and HSA) [43,44,66–84], hemoglobin [85], lysozyme [86–93], hydrophobin [94], and oleosin [95,96].

The formation of MBs with protein shells occurs not only due to physical but also chemical processes. However, it remains a challenge to figure out the primary and leading process in MB shell stabilization. The formation, growth, and collapse of MBs can occur during intense local heating, which causes a change in the secondary and tertiary structures of the protein and can also cause high-energy chemical reactions [85]. Moreover, researchers emphasize the role of the radicals formed during the reaction [97]. A study was carried out to identify which particular radical is important for obtaining stable MBs [98]: chemical traps for various types of radicals were added to the MB formation process, and the effect was monitored for the possibility of fabrication, stability, and concentration of agents. The effect of catalase, which decomposes hydrogen peroxide (H_2O_2), and superoxide dismutase, which decomposes superoxide (HO_2) [99], were tested. Superoxide dismutase blocked the formation of MBs, which presumably indicates the participation of superoxide in the reaction of MB formation. Furthermore, it is known that superoxide dismutase easily oxidizes cysteine residues present in many natural proteins used for synthesis [100].

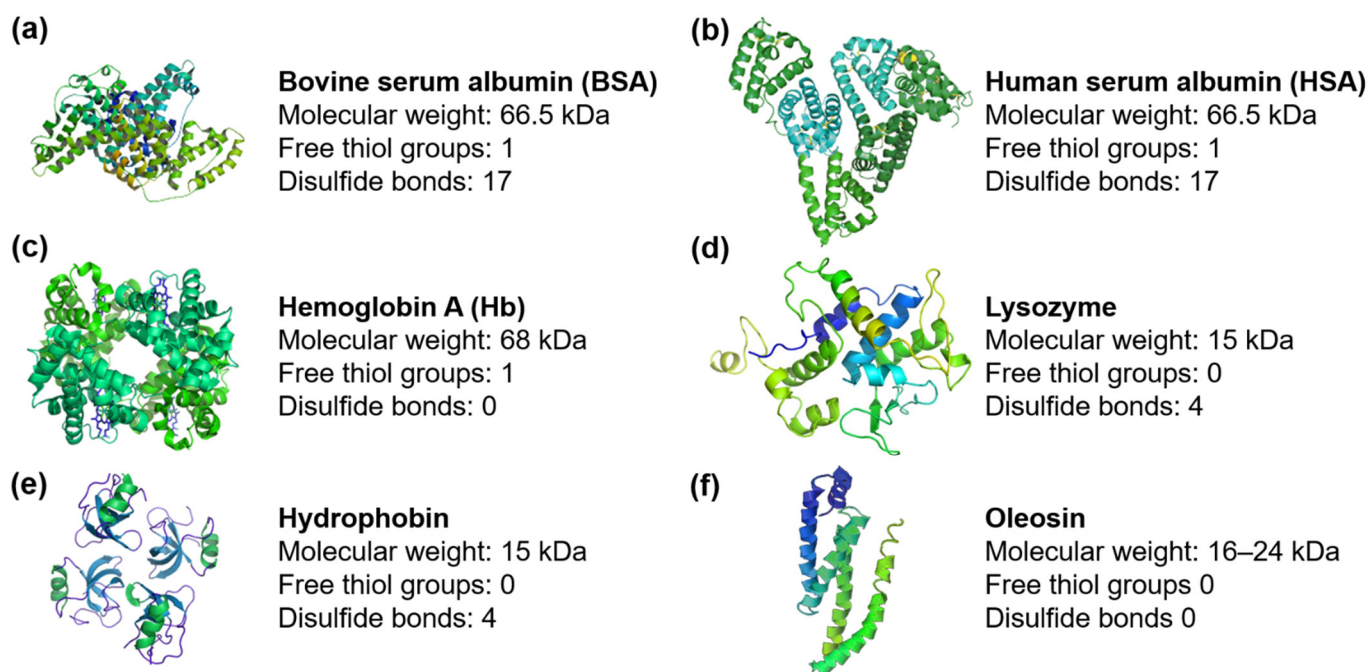


Figure 2. Proteins involved in MB shell stabilization: (a) bovine serum albumin (BSA), (b) human serum albumin (HSA), (c) hemoglobin, (d) lysozyme, (e) hydrophobin, (f) oleosin. For all proteins, characteristics such as molecular weight, numbers of free thiol groups, and disulfide bonds involved in MB formation and further functionalization, are provided.

Several studies [85,86,90–93,98] indicated that the formation and destruction of disulfide bonds play an important role in MB formation with a protein shell. Thus, in [98], hemoglobin and myoglobin were compared: the main difference between proteins is the presence of cysteines in the structure. The latter does not have thiol groups and, as shown, did not form MBs. The addition of cross-linking reagents (i.e., dithiothreitol, DTT) also has been already shown to stabilize the MB structure [66,90–93]. However, the addition of dithioerythritol, DTE, which destroys disulfide bonds or the process of alkylation of the thio-group, leads to MB destruction.

It should be noted that the energy during the reaction of MB formation is sufficient to destroy the labile existing S-S disulfide bond and form a new one. Furthermore, ref. [67] revealed an increase in the stability and concentration of agents when the protein was pretreated with the Traut's Reagent (2-iminothiolane), which provides an additional amount of thio-groups by conversion of free amino groups into thio-groups. However, many studies on protein MB formation have shown a dependence not only on the number of thio-groups but also on other possible factors (i.e., the protein structure). For example, the non-universality of the "thiol" substantiation of the MB formation mechanism can be illustrated with MBs stabilized with sulfur-free proteins, such as streptavidin [101] or oleosin [95,96]. Hence, the procedure of MB formation is selected individually for each protein, with its molecular weight, protein structure, and the number of groups that can be involved in the reaction.

All-natural proteins used have the advantage of low toxicity and high biocompatibility. In this aspect, HSA is an ideal candidate for the clinical translation of protein-based US contrast agents. In most studies, due to the high cost of HSA, its less expensive analog, BSA, is used. Its amino acid sequence is 75% identical to the molecular structure of HSA; HSA and BSA have the same molecular weight and behave similarly during MB fabrication [66,102,103]. During numerous experiments with albumin-based MBs, hypotheses about changes in the globular structure of proteins were expressed. The protein MB shell may be formed by close packing of reagents, where hydrophobic fragments of neighboring proteins are tightly packed, and the former intramolecular disulfide bonds

are rearranged into intermolecular disulfide bridges. Unfortunately, there is no explicit confirmation of the protein structure inside the shell. However, in [79], it was reported that the MB destruction time correlates with the decrease in the percentage of α -helices during synthesis, which can be considered as an indirect argument in favor of stabilization by unfolded protein molecules.

Proteins with high molecular weight, such as hemoglobin and streptavidin, are used much less frequently compared to albumins. Proteins with significantly lower molecular weights raised interest. Studies on comparing low and high molecular weight proteins (i.e., lysozymes and albumins) did not reveal significant differences in MB properties. However, conditions for MB fabrication were selected individually for each case [66,93,104]. From this perspective, lysozyme demonstrated its potential for protein MB formation due to its unique enzymatic, antibacterial activity [90–92,104]. However, the introduction of the universal protocol for the fabrication of protein MBs with desired properties is still yet to come.

3. Fabrication of MBs with Protein Shell

MB properties relevant to clinical translation (mean diameter, monodispersity, stability) are tied to the initial fabrication procedure; hence, this section summarizes known approaches to produce MBs with protein shells. Methods include a traditionally referred sonication procedure, a recently explored microfluidic approach, and four techniques designed to increase the volume of produced MBs. Schemes of fabrication routes are summarized in Figure 3.

During the sonication procedure, MBs are primarily formed due to the propagation of high-intensity US waves through a liquid resulting in a cavitation process (Figure 3a) [19,78,97,105–111]. Typically, the tip of the sonotrode is placed at the gas-liquid interface for MBs fabrication, similar to the formation of micelles, where the tip is placed at the water-oil interface. Sonication is the leading MB production method since chemical laboratories usually have the required setup. However, the method's main disadvantage is MB polydispersity, affecting their US performance [66]. Monodisperse-sized MBs can demonstrate reduced echo-to-echo decorrelation [112] and enhanced drug delivery properties [113].

Microfluidics aimed to overcome the limitation of polydispersity in MB fabrication. Another advantage of microfluidics is the precise control over reagents involved in MB fabrication. In flow-focusing devices, inner channels with a gaseous phase and outer channels with a continuous phase are merged into a small orifice, leading to MB formation. In T-junction devices, a continuous phase channel is placed perpendicular to a gas phase channel; thus, when gas penetrates the continuous phase under required pressure and flow velocity, local instability at the gas-liquid interface results in MB formation (Figure 3b) [10,114–117]. However, the scalability of MB production with microfluidics remains the main current limitation.

Coaxial electrohydrodynamic atomization (CEHDA) involves two co-flowing media subjected to a high voltage under ambient conditions to generate coaxial jetting, acting as a compromise between sonication and microfluidics with the advantage of high and scalable MB yield (Figure 3c) [118–120]. However, protein MBs are typically large-sized (40–800 μm) compared to lipid MBs [120] produced by CEHDA. Additionally, the high voltage (of 12.8 kV) applied in CEHDA might be a limitation for translation [87].

Pressurized gyration is based on centrifugal spinning and solution blowing to form nanofibers in large quantities and results in the parallel formation of many nanofibers with regular morphology (Figure 3d) [87]. Several articles considered lysozyme-based MB fabrication for biosensing and antibacterial activity [87,121]. Still, the narrowest possible mean size of MBs was only 37 μm , and additional work on expanding pressurized gyration's speed and pressure regimes are required to meet the size criteria of biocompatible agents.

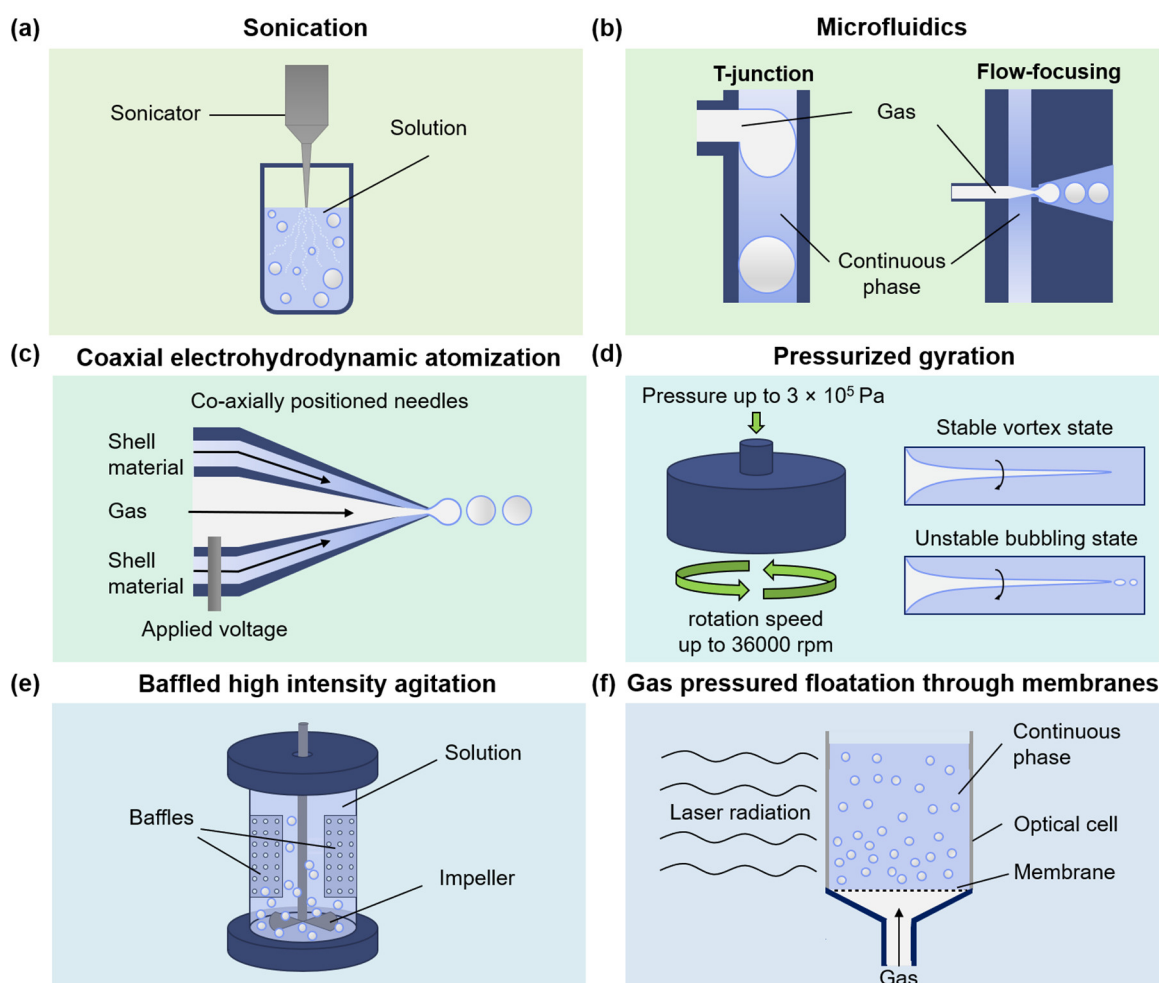


Figure 3. Strategies for protein MBs fabrication. (a) Sonication, (b) flow-focusing and T-junction microfluidics, (c) coaxial electrohydrodynamic atomization (CEHDA), (d) pressurized gyration, (e) baffled high-intensity agitation (BHIA), and (f) gas-pressured floatation through membranes.

Baffled high-intensity agitation (BHIA) cells were recently involved in MB formation. The hydrodynamic cavitation of fluid near the impeller and baffles zone at the expense of dissipating more turbulent energy leads to MB formation with sizes smaller than $10\ \mu\text{m}$, as recently shown for BSA MBs (Figure 3e) with different gases loaded in the core [70]. O_2 - and N_2 -filled MBs were stable for 16 h with mean sizes of $3.7 \pm 3.3\ \mu\text{m}$ and $4.4 \pm 2.2\ \mu\text{m}$, respectively. Interestingly, a BSA solution volume of 350 mL was used, scaling the production capabilities of protein-shelled MBs. Further work should be focused on producing narrow-sized MBs by tuning the setup or introducing size separation after MB formation.

Gas pressured floatation through membranes was also implemented for MB formation (Figure 3f): uniform-sized MBs grow at the pore openings of the inner membrane surface, and when the MB volume reaches a specific size, it detaches from the inner surface of the membrane [122,123]. Additionally, further limiting MB size to a $1\text{--}7\ \mu\text{m}$ range is required.

However, only a few methods can produce protein MBs with the sizes required for medical applications ($<7\ \mu\text{m}$) and have already gained numerous investigations: sonication (the first historically described method) and microfluidics (recently developed method for fine-tuning MB properties such as monodispersity, control over the MB yield and precise direct functionalization routes). Therefore, we will focus attention on sonication and microfluidic-based methods of MB fabrication to discuss recent advances in the field.

3.1. Sonication

A broad set of parameters of the sonication procedure of MB fabrication can be varied: preheating temperature of the initial solution, sonication time, tip location (at the gas-liquid interface or slightly deeper in the solution), US power, frequency, and time of storage for MB stabilization (Figure 3a) [10,19,66]. Since formed MBs are polydisperse in size and formed in solutions with excess reagents, size isolation and MB purification are needed. Upadhyay and Dalvi thoroughly described protein MBs fabricated by sonication in [66].

For example, BSA or HSA solutions can be heated up to 60 °C reaching 80 ± 5 °C during a procedure. The preheating of the initial solution can be used to change protein structure or lead to its denaturation. Moreover, the increasing temperature can lower the solution's surface tension and assist in forming MB with narrow size distribution [19,21]. The sonication procedure can last from 15 s to 5 min with the sonotrode power of 20–240 W and a US frequency of 20 kHz [66].

The MB size distribution can be tuned by sonication power and time of exposure during sonication [30,112]. Moreover, post-sonication promises size tuning after MB formation, as demonstrated for lysozyme MBs [93]. Narrow size distribution with post-sonication can be achieved by (i) lowering US frequency or (ii) increasing acoustic power at a fixed acoustic power.

The ease of sonication technique combined with a set of predefined parameters to control during the MB synthesis resulted in the widespread use of the method for MB fabrication. Still, MB size polydispersity remains a challenge. Therefore, a microfluidic-based approach was described recently to solve this issue.

3.2. Microfluidics

Ideal microfluidic-based fabrication may allow producing (i) MBs with predefined diameter in the range of 1–7 μm and small size polydispersity, which is relevant to advance US contrast properties, (ii) MBs with the controllable concentration needed for the procedure, which can be a crucial advantage for clinical translation of the technology [10,114–117]. With two types of microfluidic devices highlighted in Figure 3b, all known examples of protein MB microfluidic-assisted MB fabrication are listed in Table 1.

Table 1. Fabrication of MBs with protein shell by microfluidics. All examples within each type of microfluidic device are provided in chronological order.

Microfluidics Type	Primary Shell Material	Additives	Gaseous Core	Size (μm)	Ref.
Flow-focusing	BSA (3%, 5%)	None/ Dextrose/Glycerol, propylene glycol, and isotonic saline	N ₂	10–20	[124]
	Oleosin	Pluronic F68/Pluronic F127	N ₂ , C ₄ F ₈	3.9 \pm 0.2	[125]
	BSA (3%)	Dextrose (10%)	N ₂	9.1–19.8	[126]
	BSA (4%)	Dextrose (10%)	N ₂	9.8 \pm 0.3–31.1 \pm 1.4	[127]
	Oleosin	Pluronic F68/Pluronic F77/ Pluronic F105/ Pluronic P65	N ₂	2–4	[95]
	Oleosin	Pluronic F68, Methylene Blue	N ₂	2–4	[96]
T-junction	BSA (15%)	None/ Tween 40/phospholipid solution	Air	81 \pm 2–555 \pm 3	[128]
	BSA (15%)	-	N ₂	272 \pm 5	[129]
	BSA (15%)	None/Glutaraldehyde (0.75%)	N ₂	270 \pm 2	[79]

The pioneering work on protein MB fabrication with microfluidics was reported in 2013 by Chen et al.: the flow-focusing device produced agents with BSA or blood plasma shell [124]. Plain protein MBs tended to coalesce rapidly; hence, surfactants (such as dextrose) tuned MB storage stability. The authors demonstrated a step toward MB

fabrication with patient blood material; however, the mean diameter was greater than the optimal range of 1–7 μm [124]. Later, the approach that combined MB fabrication and direct administration into a mouse tail vein was performed by Dhanaliwala et al. [126]. Moreover, they demonstrated sonothrombolysis in vitro enhancement when a device was placed in situ adjacent to the clot [127].

Another strategy was proposed by Angilè et al., combining Oleosin with nonionic triblock copolymers poloxamers (i.e., Pluronic F68) [125]. While pure oleosin MBs were larger than 10 μm , the introduction of poloxamers tuned the diameter to 4 μm by lowering the surface tension of initial solutions. Next, tailoring of US response was performed by variation of amphiphilic copolymers in the MB shell: the introduction of longer hydrophilic domains of poloxamers allowed to increase MB shell stiffness [95]. Produced MBs had a diameter of 2–4 μm , were stable over two weeks, and were comparable to commercially available US contrast agents. Later, they produced the bimodal US and photoacoustic agent. Simple electrostatic interactions between oleosin and methylene blue successfully functionalized MBs directly within the microfluidic chamber [96].

Compared to flow-focusing devices, T-junction microfluidic devices produced albumin-shelled MBs with relatively larger diameters of 80–550 μm [79,128,129]. Therefore, flow-focusing devices can produce protein MBs with clinically-relevant properties of size, MB yield, and storage stability.

Therefore, the ideal procedure for protein MB fabrication should offer (i) narrow MB size distribution within the range of 1–7 μm combined with a high MB yield and (ii) demonstrate scalability for the industry implementation combined with ease of implementation. The sonication procedure demonstrates a lack of size monodispersity, microfluidics in the current state is a hardly scalable route for MB production at an industrial scale. However, one of the promising solutions can be direct MB fabrication within a hospital in amounts needed for the department needs, where sonication, microfluidics, and BHIA could be adapted. Moreover, precise attention to the interface phenomena during MB fabrication (i.e., surface tension) could optimize fabrication strategies.

4. Chemical Routes for Stabilization and Functionalization of MBs with Protein Shell

Protein-based MB functionalization is carried out in two directions: (1) to prolong agent stability (i.e., storage stability, circulation time) and (2) to achieve multifunctionality for applications beyond US imaging. Incorporation of additives into MB shell (noble metal nanoparticles, polymeric nanoparticles, nucleic acids, functional dyes, proteins, and antibodies) expands MB applications to fields of photoacoustic imaging, (targeted) drug/gene delivery, chemo- and photodynamic therapy, antibacterial activity, and even biosensing (Figure 4a).

4.1. Prolonged Stability

Two approaches are generally used to achieve prolonged MB stability (Figure 4a). In the first case, active molecules are added during the MB fabrication procedure, contributing to the additional chemical crosslinking of proteins in the MB shell. Several works demonstrated that the addition of reagents having both hydrophobic and hydrophilic fragments in their structure contributes to a denser packing of the MB shell and, consequently, increased stability. For example, Upadhyay et al. [73] produced BSA MBs introducing caprylic acid and N-acetyl-DL-tryptophan in various ratios. Spectroscopic analyses of fluorescence and circular dichroism demonstrated the influence of additives and synthesis conditions on the secondary and tertiary structure of the protein. The use of tryptophan in the MB formulation contributes to the enhanced deployment of BSA molecules, resulting in MBs with a shelf life of up to 8 months at 4 °C, which is comparable to the shelf life of polymeric MBs [73,130]. Prolonged stability can be described by forming intermolecular disulfide bonds in the MB shell. In the works [86,90,93,101], a method involved DL-dithiothreitol or β -mercaptoethanol to reduce disulfide bonds and form free thio- groups for later intermolecular coupling. The number of thio- groups can also be

increased with the Traut's reagent [67]: the amino groups included in the protein structure (lysine and arginine) interact with the reagent resulting in the formation of active thio-groups. Another approach involved the covalent crosslinking of proteins with glutaraldehyde as a crosslinking agent [80,109]. The use of such reagents increases stability and circulation time. Additionally, the narrow size distribution of MBs can be achieved.

In another case, the stability is increased by adding a reagent as an additional MB shell layer or as an intermolecular "holding" reagent. In several works, carbohydrates (dextrose and analogs) were involved in protein MB stabilization, a strategy known as "PESDA" [73,74,78,111,124]. Here stabilization occurs due to electrostatic interactions; similar interactions occur with introducing glycerol and ethylene glycols [124,131]. In [74], the strategy of the covalent introduction of polyethylene glycol by carbodiimide binding to the carboxyl group of the protein resulted in desired stability properties of protein MBs. Similarly, in [86], MBs were covalently modified using pre-oxidized dextran followed by the interaction of the aldehyde group with the amino group of the protein.

Several works considered the implementation of Layer-by-Layer assembly on the protein MBs (Figure 4a) [75,77,109,132,133]: unfortunately, this strategy tended to decrease MB concentration and even stability with the addition of each layer. Only one to two layers were sufficient to balance prolonged stability and the further ability for functionalization (which is also possible directly using amino and carboxy groups in the protein).

4.2. Advanced Functionality

Two types of interactions can be distinguished for introducing functional groups onto protein MBs: non-covalent (key-lock, electrostatic, or hydrophobic interactions) and covalent (Figure 4b).

The key-lock interactions are widely known by the biotin-avidin (or biotin-streptavidin) interactions. Either biotin fragments [82] or protein [71] are typically introduced into the MB structure, and then efficient coupling is carried out on the MB interface. This approach is directly used for the introduction of antibodies. However, electrostatic binding is the most widespread due to ease of implementation and the presence of positively and negatively charged groups in the protein structure. The elimination of the functional group is the most effective route due to the lack of loss of functional properties. This approach was demonstrated for the introduction of active molecules (i.e., ascorbic acid [134], cysteine [135], nucleic acids or synthetic oligonucleotides [81,131,136], antibodies, enzymes and other peptides [68,73,74,86]), and gold nanoparticles with different morphology [19,21,71,137].

Covalent binding is typically carried out with carbodiimide synthesis or by introducing additional crosslinking reagents. Attachment of antibodies [89] and nanoparticles containing nucleic acids [80] was implemented by maleimide and glutaraldehyde, respectively. Liu et al. [83,84] demonstrated the option of click reaction for MB functionalization since click reaction is highly efficient to incorporate a broad set of additives (nanoparticles, siRNA, antibodies).

Therefore, the chemistry behind MB functionalization involves a predefined set of strategies to implement. Furthermore, the presence of amino acids with different radicals in the structure of protein MBs allows for quick incorporation of the necessary functional fragments into MB structure. Hence, protein MBs can act as efficient agents for multimodal imaging and image-guided therapy applications.

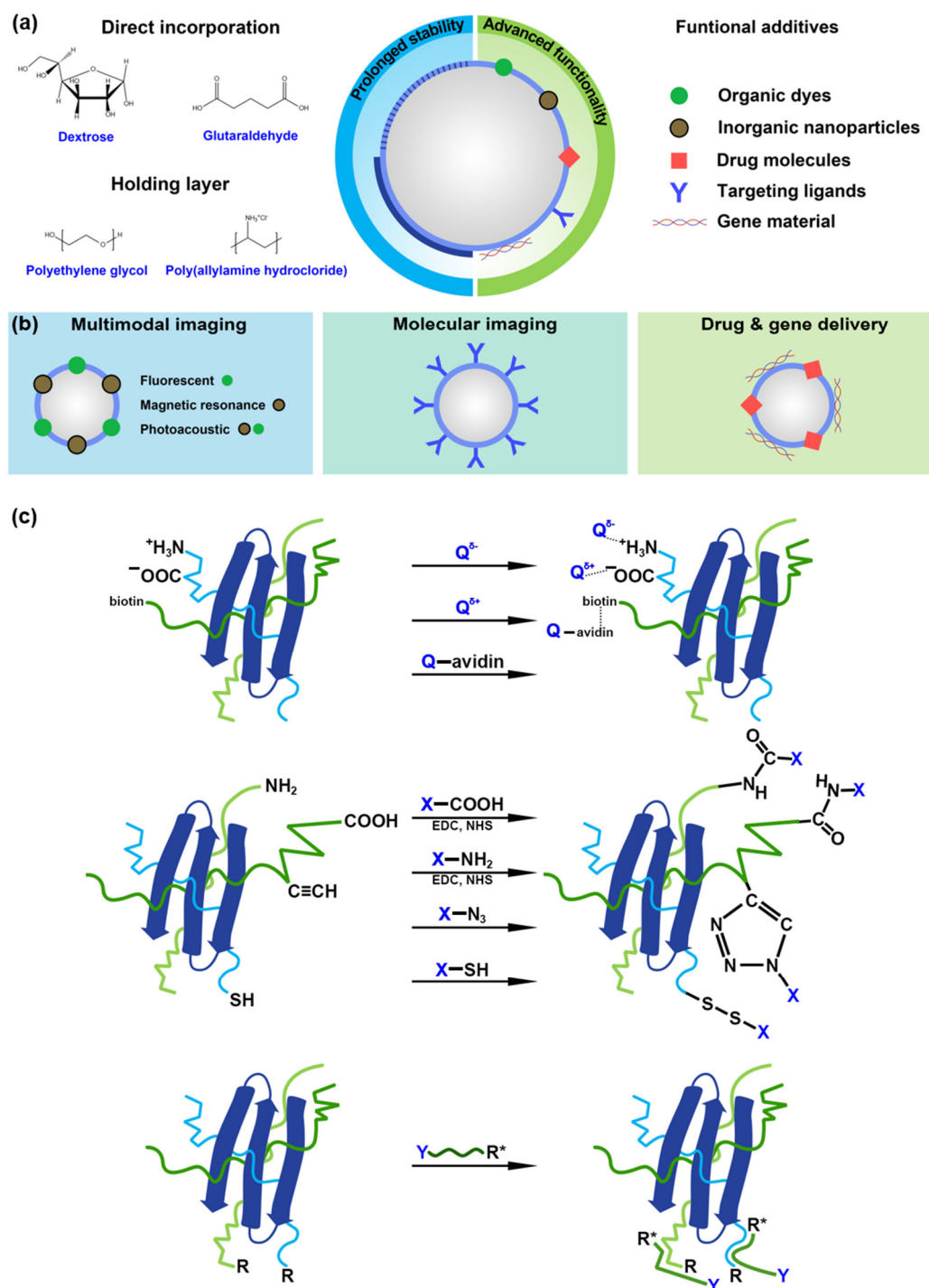


Figure 4. Chemical routes for stabilization and functionalization of MBs with protein shell. (a) Prolonged stability of protein MBs can be achieved with direct incorporation of stabilizers (i.e., dextrose or glutaraldehyde) or with the implementation of a “holding” layer of poly(ethylene glycol) or poly(allylamine hydrochloride), while advanced functionalization offers the opportunity to incorporate a broad set of functional additives; (b) The proper choice of functional additives results in MB applications for multimodal imaging (where gaseous core provided US imaging, while dyes or nanoparticles provided additional fluorescent/magnetic resonance/photoacoustic modality), molecular imaging (due to targeting ligands), and drug/gene delivery (with functional payloads); (c) Schematic representation of chemical routes for protein MB functionalization with non-covalent (electrostatic and “key-lock” with biotin-avidin pair) or covalent interactions (primarily by carbodiimide synthesis or with the introduction of additional crosslinking reagents), as well as hydrophobic interactions.

5. Advanced Characterization of MBs with a Protein Shell

The expedient choice of characterization method is essential to fully evaluate the properties of protein MBs, as recently demonstrated for dye-labeled BSA MBs [138]. In this section, we summarize existing approaches in MB characterization, providing examples in Figure 5.

After MB fabrication, size distribution and concentration properties must be evaluated first. MB size can directly affect their US response, while high and monodisperse MB yield raises the reasonability of agent production [139,140]. Few measurement approaches could be considered. The traditional one is based on combining optical microscopy (OM) with a cell counter, where MBs are counted manually in a time-consuming manner [19,21,90,138,141,142]. Another approach involves Coulter counter (CC) measurements, based on resistive pulse sensing for counting and sizing particles suspended in electrolytes. The CC device reduces the quantification time significantly [20]. In contrast, two light scattering-based methods, dynamic light scattering (DLS) and nanoparticle tracking analysis (NTA), can be considered. However, both methods result in distorted size distribution due to initial high MB size polydispersity. Moreover, it should be noted that the accuracy of measurements is strongly dependent on sample dilution [143,144]. Therefore, CC measurements are more favorable than other methods in terms of ease of operation and reliability of obtained results.

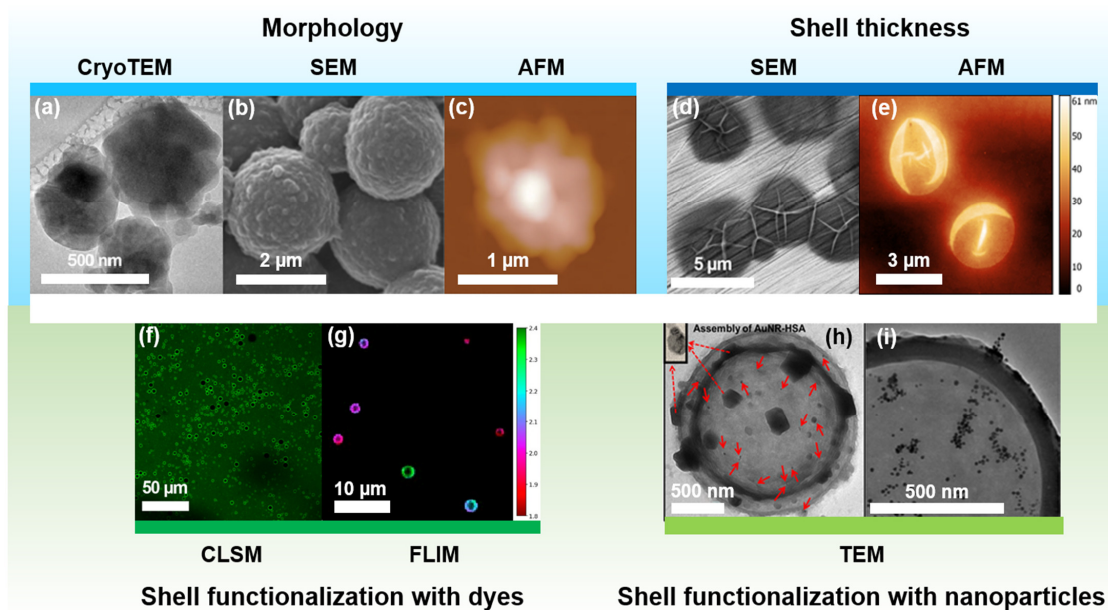


Figure 5. Characterization of MBs with a protein shell: methods to evaluate morphology, shell thickness, and functionalization of fabricated agents. Morphology evaluation: (a) CryoTEM image of BSA MBs; (b) SEM image of modified lysozyme MBs. Adapted with permission from Ref. [89]. Copyright 2013, American Chemical Society; (c) AFM image of lysozyme MBs. Adapted with permission from Ref. [133]. Copyright 2008, American Chemical Society; Shell thickness measurements: (d) SEM and (e) AFM images of BSA MBs were used to evaluate shell thickness; confirmation of shell functionalization with dyes: (f) CLSM and (g) FLIM images of rhodamine-labeled BSA MBs; Confirmation of shell functionalization with nanoparticles: (h) TEM image of gold nanorods (AuNRs) functionalized HSA MBs. Adapted with permission from Ref. [145]. Copyright 2012, SPIE; (i) TEM image of gold nanoparticles (AuNPs) functionalized lysozyme MBs. Adapted with permission from Ref. [89]. Copyright 2013, American Chemical Society. Abbreviations: cryoTEM, transition electron cryomicroscopy; SEM, scanning electron microscopy; AFM, atomic force microscopy; CLSM, confocal laser-scanning microscopy; FLIM, fluorescence lifetime imaging microscopy; TEM, transition electron microscopy. Where red arrows indicate single AuNRs and dashed ones point to assemblies of AuNR and HSA.

For characterization of MB morphology, transmission electron cryomicroscopy (TEM), scanning electron microscopy (SEM), and atomic force microscopy (AFM) methods were successfully implemented, examples are provided in Figure 5a–c, respectively [94,133,145,146]. SEM of broken MBs and AFM of dried MBs can provide precise information about MB shell thickness, as illustrated in Figure 5d,e, respectively [90,146]. AFM of liquid samples can shed light on MB shell stiffness profile, acting as the only method for Young modulus evaluation of MB shell [146]. However, only a few articles considered AFM for MB characterization due to the MB fragility and sophisticated sample preparation route.

The introduction of fluorescent small molecules can be confirmed by confocal microscopy (Figure 5f) [84,109,133,143,147], while STED or fluorescent lifetime imaging microscopy (FLIM) may offer higher image resolution combined with insight into the homogeneous/heterogeneous distribution of fluorescent components in the shell and distribution of dye among MB population (Figure 5g) [148]. Unfortunately, FLIM and STED methods are barely described for protein MBs [138]. The presence of inorganic nanoparticles can be confirmed with TEM (Figure 5h,i) [89,145]. MB drug loading capabilities are usually evaluated with spectrophotometry or chromatography [20].

The storage stability of protein MBs can be evaluated by zeta-potential measurements, in addition to methods described for size/concentration characterization [19,70,109,138,149]. However, significant attention should be given to the stability of MBs in blood-mimicking solutions, resulting in the evaluation of a parameter similar to in vivo circulation time. It can be done with vessel-mimicking phantoms with predefined pumping speed. Similar phantoms are generally constructed to evaluate the acoustic response of fabricated MBs.

Therefore, a straightforward strategy to assess fluorescent drug-loaded protein MBs (i.e., doxorubicin-loaded HSA MBs, as clinically-relevant anticancer formulation) could be: (1) to characterize the size and concentration via CC, (2) to assess morphology and drug loading using STED or FLIM and spectrophotometry, (3) to evaluate stability and acoustic response in vessel mimicking phantom and the solution mimicking blood composition.

6. Applications of MBs with Protein Shell beyond US Imaging

Historically, MBs entered clinical practice as US contrast agents. Over the past 20 years, the research interest in MBs shifted from US imaging to combined image-guided/multifunctional strategies. In addition to US imaging, MBs gained applications in photoacoustic (PA) imaging, targeted and image-guided drug or gene delivery, antibacterial activity, and biosensing, as schematically represented in Figure 6. This section provides all known options for multifunctional applications of protein-based MBs.

6.1. Imaging Applications

PA and US are complementary imaging methods since both strategies receive acoustic echo to construct resulting images. In addition, absorbers, such as organic dyes or plasmonic nanoparticles, can tune the resulting PA images (as MBs for US imaging). The introduction of dyes into the MB structure has been known for a long time [72]. Recently, the introduction of PA dyes, such as methylene blue [96] or indocyanine green [19], has been demonstrated. Furthermore, it has been shown that US and PA signals can be controlled independently by changing the dye concentration in the MB structure, which was confirmed by in vivo studies. Such examples may represent promising bimodal agents for brain imaging or sentinel lymph node detection (Figure 6) [150–154].

Beyond US cardiac imaging, protein-shelled MBs can be used for imaging the endothelium [72], vessels with atherosclerotic plaques [110,111], and detection of inflammatory foci (Figure 6) [69,72]. It has been shown that MBs do not adhere to normal human endothelial cells but can adhere to inflamed lesions. We may name several reasons for this effect. Endothelial cell surface proteins, such as leukocyte adhesion molecules, are activated and expressed during inflammation [155–157]. Hence, they may have an affinity for protein MBs through protein-protein interaction. Furthermore, the inflammatory response includes

the synthesis of new matrix components and the degradation of pre-existing ones [158]. Thus, matrix degradation products also may show an affinity for MBs. It is also possible that albumin in the bladder membrane is involved in adhesion because albumin binds *in vivo* to the endothelial glycocalyx via at least four putative albumin-binding proteins [159,160]. Moreover, endothelial damage can occur due to a variety of causes: arterial hypertension, hyperlipidemia, diabetes mellitus, coronary angioplasty, or postischemic reperfusion, and result in atherosclerosis, thrombosis, or restenosis [161–163]. Early atherosclerotic lesions and predisposition to thrombosis coincide with endothelial cell protein activation and leukocyte adhesion molecules activation [161,164,165]. Thus, MBs with the protein shell have an advantage for early detection of inflammation due to the mentioned reasons. MB-endothelial adhesion could eventually be extended to developing contrast agents that target specific markers of the cellular phenotype, opening up opportunities for tissue-specific contrast US imaging.

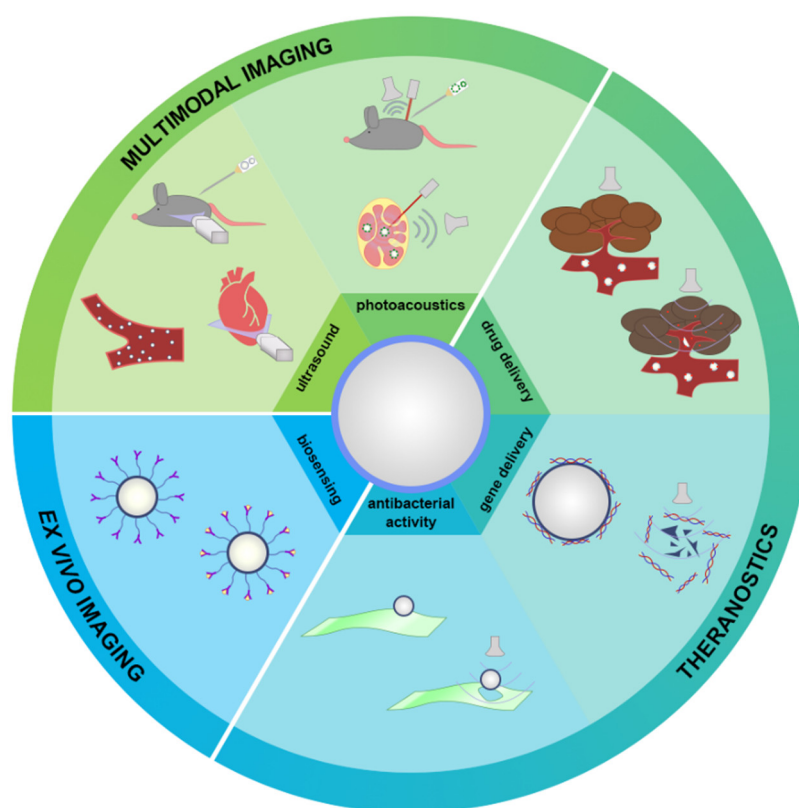


Figure 6. Applications of MBs with protein shell. Historically, protein MBs were the first contrast agent for cardiac US imaging, while recent advances in photoacoustic imaging expanded their multimodal imaging applications. Theranostic strategies result in US-assisted drug and gene delivery and antibacterial purposes based on US-assisted MB destruction. Ex vivo imaging purposes demonstrated with MB-assisted biosensing can widen the range of MB applications.

6.2. Drug/Gene Delivery

Protein MBs are widely involved in cancer treatment strategies. In [71], albumin MBs with gold nanoparticles (as plasmonic nanoparticles) and VEGFR2 antibodies (as targeting ligands) adsorbed on the surface were used for targeted photothermal therapy. After binding to angiogenesis markers, MBs were sonicated to release the therapeutic agent confirmed by PA measurements. Yoon et al. [137] also used gold nanoparticles prone to aggregation: after US-mediated MB destruction, nanoparticles entered tumor lesions via sonoporation and aggregated. Then, photothermal therapy was applied. In addition, photodynamic therapy can be optimized with MBs since it is relevant to deliver not only photodynamic agents but also oxygen (since hypoxic conditions occur in

tumors typically), while photodynamic agents can be delivered to the tumor site with sonoporation [166–169]. Previously, photodynamic dyes (indocyanine green, zinc phthalocyanine) and gold nanoparticles were implemented on the albumin MB shell [19,21]. Narihita et al. [68] developed albumin MBs coated with cetuximab for theranostics of oral squamous cell carcinoma (HSC-2). The cell killing rate during sonication in the presence of cetuximab was higher than for non-targeted albumin MBs. On the other hand, selective cell killing was not observed in the human myelomonocytic lymphoma line (U937) with no cetuximab affinity. Another anticancer drug, doxorubicin, was used for protein MB formulation in [104,170,171]. Due to hydrophobic interactions, drug molecules were sorbed on lysozyme MBs, and MBs showed promising treatment results. Thus, protein-based MBs can potentially be used for theranostics as drug delivery vehicles, enhancing therapeutic effects in cancer treatment (Figure 6).

Several studies have shown that albumin MBs can effectively bind nucleic acids and synthetic oligonucleotides (Figure 6) [172]. MBs can directly capture genetic material such as plasmids and adenoviruses. The first published report on targeted DNA delivery was performed in 1996 using intravenously delivered MBs containing oligonucleotides [53]. In 1997, Bao et al. [173] described the use of US and albumin-coated MBs to enhance transfection of the luciferase reporter plasmid in cultured hamster cells. Shohet et al. [174] demonstrated that US-mediated destruction of gas-filled MBs can be used for direct gene expression to the heart in vivo. Intravenously administered recombinant adenoviral vectors encoding the beta-galactosidase reporter gene were successfully delivered to normal rat myocardium using MBs and a 1.3 MHz transthoracic diagnostic US device with a mechanical index of 1.5. Of note, no transfection was observed if adenovirus was administered at the same dose without MBs or if adenovirus was administered with MBs, but US was not applied [175]. Nowadays, many studies have confirmed the effectiveness of US-mediated MB destruction for both in vitro and in vivo drug and gene delivery [80,81,109,136,174,176,177].

6.3. Antibacterial Activity

In 1922, before discovering penicillin, Alexander Fleming discovered that lysozyme inhibits bacterial growth [178]. Lysozyme is a natural enzyme found in body secretions such as tears, saliva, and milk and is considered part of the innate immune system of most mammals [179]. Lysozyme destroys peptidoglycan in the bacterial cell wall, leading to cell death [180]. Lysozyme was already used to form MBs [93]. Lysozyme MBs can also partially retain their antimicrobial activity despite changing protein conformation (Figure 6) [133].

Hence, Mahalingham et al. [87,121] demonstrated the antibacterial activity of lysozyme-based microbubbles against Gram-negative *Escherichia coli* (*E. coli*). Another study [88] investigated a novel strategy for acne treatment based on the antibacterial action of lysozyme MBs and US-mediated cavitation both in vitro and in vivo, aiming to reduce the dose and duration of treatment. As a result, the growth of *P. acnes* bacteria was inhibited by $86.08 \pm 2.99\%$. Furthermore, MBs can have not only antibacterial but also antimicrobial activity [89]: the introduction of gold nanoparticles in the MB structure can exhibit antimicrobial activity and demonstrate effectiveness against *M. lysodeikticus*.

6.4. Biosensing

Biosensing is an intriguing MB application beyond in vivo imaging and therapy (Figure 6). While many cell sorting techniques were already described, including fluorescence-activated or magnetic field-activated ones, mechanical forces can damage cells during a procedure. Liou et al. [82] demonstrated the MB-assisted method, buoyancy-activated cell sorting, which involves MBs composed of biotinylated albumin conjugated to anti-CD44 antibodies. MBs were implemented to isolate breast cancer cells, and over 90% of the cells were collected in the microbubble layer. CD44+ is a widely used cancer stem cell biomarker. Thus, the described agents could be a powerful tool for sorting cancer stem cells from dissected tumor tissue. Another option of MBs used as biosensors was described in [89].

The interface of the lysozyme-based MBs was modified with alkaline phosphatase to detect the presence of paraoxon in aqueous solutions at the lowest concentrations down to 1 ppm.

Thus, the range of applications of protein-based MBs covers not only US imaging but also other imaging and therapeutic strategies and biosensing options. These strategies directly depend on the MB structure: gaseous core, a primary protein used for shell stabilization, and functional additives.

7. Conclusions

Protein MBs are still clinically available US contrast agents with the example of Optison with the HSA-stabilized shell. HSA is considered the most well-discovered protein with clear perspectives for clinical translation of HSA-based solutions. Hence, HSA-stabilized MBs can be produced with a concentration up to 10^{10} MBs/mL, tuned mean diameter in the range of 1–7 μm , and circulation time of 1–2 min [20,48,49,53–55]. However, the introduction of stabilizing agents in the BSA shell of agents can improve properties of low stability and short circulation time [80,109]. Moreover, large-scale production of monodispersed HSA MBs, a few microns in mean diameter, remains a point for improvement [79,128,129]. Beyond albumin, oleosin (recently involved in microfluidic narrow-sized MB fabrication) [95,96] and lysozyme (with advantages in antibacterial activity and biosensing) [87,89,121] are the most relevant proteins for MB production.

Therefore, MBs with the protein shell demonstrates a predefined set of proteins used for shell stabilization, as well as fabrication routes aimed at large-scale production; well-discovered functionalization routes (non-covalent as electrostatic, hydrophobic, “key-lock” interactions or covalent, by carbodiimide synthesis or with the introduction of additional crosslinking reagents) [80,82,134], and a broad set of biomedical applications (anticancer therapy, drug/gene delivery, antibacterial activity, and biosensing) [19,71,87,89,96,121]. Hence, protein MBs are superior platforms for the practical translation of smart agents.

Further research should be considered on the topics of:

(1) Systematic evaluation of strategies to prolong protein MB stability (both storage stability and stability during imaging/treatment procedure) with the precise attention to biocompatible additives that can be easily incorporated into MB shell and can shift MB shell properties to hard as polymer MBs;

(2) Large-scale production of functional MBs with narrow size distribution and high production yield involving predefined routes for MB functionalization directly during MB fabrication;

(3) Critical evaluation of MB behavior under conditions close to natural for a better understanding of their efficiency in practical clinical applications in imaging and therapy and reasonable design of smart agents;

(4) Further exploration of MB applications for biological barriers opens research on brain disorders, transdermal drug delivery, and smart anticancer therapy [170,181–186].

US-sensitive stimuli-responsive MBs open the door for advanced cancer treatment and biosensing procedures based on the effects of US-mediated MB destruction, sonoporation, and sonopermeation. Thus, combining US-guided strategies and protein MB advantages (mostly by protein-protein interactions) can lead to optimal procedures relevant for clinical practice in the short term.

Author Contributions: Conceptualization, R.A.B., P.G.R. and D.A.G.; methodology, P.G.R. and R.A.B.; data curation, P.G.R. and R.A.B.; writing—original draft preparation, P.G.R. and R.A.B.; writing—review and editing, E.P.F., A.N.S. and D.A.G.; visualization, P.S.K., R.A.B. and P.G.R.; supervision, D.A.G.; funding acquisition, P.G.R. All authors have read and agreed to the published version of the manuscript.

Funding: This work was supported by the Russian Science Foundation (grant no. 21-73-10254).

Institutional Review Board Statement: Not applicable.

Informed Consent Statement: Not applicable.

Data Availability Statement: No new data were created or analyzed in this study. Data sharing is not applicable to this article.

Acknowledgments: This work was supported by the Russian Science Foundation (grant no. 21-73-10254). The authors would like to thank Polina A. Demina for examples of cryoTEM MB images, Ekaterina S. Prikhozhenko and Daniil N. Bratashov for the example of AFM MB image; Olga A. Sindeeva for the example of CLSM MB image; Alexey V. Gayer and Evgeny A. Shirshin for the example of FLIM MB image.

Conflicts of Interest: The authors declare no conflict of interest.

Abbreviations

AFM, atomic force microscopy; BHIA, baffled high-intensity agitation; BSA, bovine serum albumin; CC, Coulter counter; CEHDA, coaxial electrohydrodynamic atomization; CEUS, contrast-enhanced ultrasound; CLSM, confocal laser-scanning microscopy; cryoTEM, transition electron cryomicroscopy; DLS, dynamic light scattering; FDA, the Food and Drug Administration; FLIM, fluorescence lifetime imaging microscopy; HSA, human serum albumin; MBs, microbubbles; NTA, nanoparticle tracking analysis; OM, optical microscopy; PA, photoacoustic; SEM, scanning electron microscopy; STED, stimulated emission depletion microscopy; TEM, transition electron microscopy; US, ultrasound.

References

1. Mitragotri, S. Healing sound: The use of ultrasound in drug delivery and other therapeutic applications. *Nat. Rev. Drug Discov.* **2005**, *4*, 255–260. [[CrossRef](#)] [[PubMed](#)]
2. Wells, P.N.T. Ultrasound imaging. *Phys. Med. Biol.* **2006**, *51*, R83. [[CrossRef](#)] [[PubMed](#)]
3. NHS England and NHS Improvement Diagnostic Imaging Dataset Statistical Release. Available online: <https://www.england.nhs.uk/statistics/wp-content/uploads/sites/2/2020/01/Provisional-Monthly-Diagnostic-Imaging-Dataset-Statistics-2020-01-23.pdf> (accessed on 1 April 2022).
4. Smith-Bindman, R.; Miglioretti, D.L.; Larson, E.B. Rising use of diagnostic medical imaging in a large integrated health system. *Health Aff.* **2008**, *27*, 1491–1502. [[CrossRef](#)] [[PubMed](#)]
5. Smith-Bindman, R.; Kwan, M.L.; Marlow, E.C.; Theis, M.K.; Bolch, W.; Cheng, S.Y.; Bowles, E.J.A.; Duncan, J.R.; Greenlee, R.T.; Kushi, L.H.; et al. Trends in Use of Medical Imaging in US Health Care Systems and in Ontario, Canada, 2000–2016. *J. Am. Med. Assoc.* **2019**, *322*, 843–856. [[CrossRef](#)]
6. Lieu, D. Ultrasound physics and instrumentation for pathologists. *Arch. Pathol. Lab. Med.* **2010**, *134*, 1541–1556. [[CrossRef](#)]
7. Aldrich, J.E. Basic physics of ultrasound imaging. *Crit. Care Med.* **2007**, *35*, 131–137. [[CrossRef](#)]
8. Cosgrove, D. Ultrasound contrast agents: An overview. *Eur. J. Radiol.* **2006**, *60*, 324–330. [[CrossRef](#)]
9. Wheatley, M.A.; Schrope, B.; Shen, P. Contrast agents for diagnostic ultrasound: Development and evaluation of polymer-coated microbubbles. *Biomaterials* **1990**, *11*, 713–717. [[CrossRef](#)]
10. Mujtaba, J.; Liu, J.; Dey, K.K.; Li, T.; Chakraborty, R.; Xu, K.; Makarov, D.; Barmin, R.A.; Gorin, D.A.; Tolstoy, V.P.; et al. Micro-Bio-Chemo-Mechanical-Systems: Micromotors, Microfluidics, and Nanozymes for Biomedical Applications. *Adv. Mater.* **2021**, *33*, 2007465. [[CrossRef](#)]
11. Paefgen, V.; Doleschel, D.; Kiessling, F. Evolution of contrast agents for ultrasound imaging and ultrasound-mediated drug delivery. *Front. Pharmacol.* **2015**, *6*, 197. [[CrossRef](#)]
12. Kooiman, K.; Vos, H.J.; Versluis, M.; de Jong, N. Acoustic behavior of microbubbles and implications for drug delivery. *Adv. Drug Deliv. Rev.* **2014**, *72*, 28–48. [[CrossRef](#)] [[PubMed](#)]
13. Stride, E.; Segers, T.; Lajoie, G.; Cherkaoui, S.; Bettinger, T.; Versluis, M.; Borden, M. Microbubble Agents: New Directions. *Ultrasound Med. Biol.* **2020**, *46*, 1326–1343. [[CrossRef](#)] [[PubMed](#)]
14. Ingram, N.; McVeigh, L.E.; Abou-Saleh, R.H.; Batchelor, D.V.B.; Loadman, P.M.; McLaughlan, J.R.; Markham, A.F.; Evans, S.D.; Coletta, P.L. A Single Short ‘Tone Burst’ Results in Optimal Drug Delivery to Tumours Using Ultrasound-Triggered Therapeutic Microbubbles. *Pharmaceutics* **2022**, *14*, 622. [[CrossRef](#)] [[PubMed](#)]
15. Rousou, C.; de Maar, J.; Qiu, B.; van der Wurff-Jacobs, K.; Ruponen, M.; Urtti, A.; Oliveira, S.; Moonen, C.; Storm, G.; Mastrobattista, E.; et al. The Effect of Microbubble-Assisted Ultrasound on Molecular Permeability across Cell Barriers. *Pharmaceutics* **2022**, *14*, 494. [[CrossRef](#)] [[PubMed](#)]
16. Langeveld, S.A.G.; Meijlink, B.; Beekers, I.; Olthof, M.; van der Steen, A.F.W.; de Jong, N.; Kooiman, K. Theranostic Microbubbles with Homogeneous Ligand Distribution for Higher Binding Efficacy. *Pharmaceutics* **2022**, *14*, 311. [[CrossRef](#)] [[PubMed](#)]
17. Hernot, S.; Klibanov, A.L. Microbubbles in ultrasound-triggered drug and gene delivery. *Adv. Drug Deliv. Rev.* **2008**, *60*, 1153–1166. [[CrossRef](#)] [[PubMed](#)]

18. Barmin, R.A.; Rudakovskaya, P.G.; Chernyshev, V.S.; Guslyakova, O.I.; Belcov, P.A.; Obukhova, E.N.; Gayer, A.V.; Shirshin, E.A.; Gorin, D.A. Optoacoustic/Fluorescent/Acoustic Imaging Probe Based on Air-Filled Bubbles Functionalized with Gold Nanorods and Fluorescein Isothiocyanate. *ACS Omega* **2021**, *6*, 3809–3821. [[CrossRef](#)]
19. Barmin, R.A.; Rudakovskaya, P.G.; Gusliakova, O.I.; Sindeeva, O.A.; Prikhozhenko, E.S.; Maksimova, E.A.; Obukhova, E.N.; Chernyshev, V.S.; Khlebtsov, B.N.; Solovev, A.A.; et al. Air-filled bubbles stabilized by gold nanoparticle/photodynamic dye hybrid structures for theranostics. *Nanomaterials* **2021**, *11*, 415. [[CrossRef](#)]
20. Liu, M.; Dasgupta, A.; Qu, N.; Rama, E.; Kiessling, F.; Lammers, T. Strategies to Maximize Anthracycline Drug Loading in Albumin Microbubbles. *ACS Biomater. Sci. Eng.* **2021**. [[CrossRef](#)]
21. Maksimova, E.A.; Barmin, R.A.; Rudakovskaya, P.G.; Sindeeva, O.A.; Prikhozhenko, E.S.; Yashchenok, A.M.; Khlebtsov, B.N.; Solovev, A.A.; Huang, G.; Mei, Y.; et al. Air-Filled Microbubbles Based on Albumin Functionalized with Gold Nanocages and Zinc Phthalocyanine for Multimodal Imaging. *Micromachines* **2021**, *12*, 1161. [[CrossRef](#)]
22. Himuro, S. Physicochemical characteristics of microbubbles. *Chem. Eng. Jpn.* **2007**, *71*, 165–169.
23. Koczera, P.; Appold, L.; Shi, Y.; Liu, M.; Dasgupta, A.; Pathak, V.; Ojha, T.; Fokong, S.; Wu, Z.; van Zandvoort, M.; et al. PBCA-based polymeric microbubbles for molecular imaging and drug delivery. *J. Control. Release* **2017**, *259*, 128–135. [[CrossRef](#)] [[PubMed](#)]
24. Shchukin, D.G.; Köhler, K.; Möhwald, H.; Sukhorukov, G.B. Gas-filled polyelectrolyte capsules. *Angew. Chemie Int. Ed.* **2005**, *44*, 3310–3314. [[CrossRef](#)] [[PubMed](#)]
25. Fokong, S.; Siepmann, M.; Liu, Z.; Schmitz, G.; Kiessling, F.; Gätjens, J. Advanced Characterization and Refinement of Poly N-Butyl Cyanoacrylate Microbubbles for Ultrasound Imaging. *Ultrasound Med. Biol.* **2011**, *37*, 1622–1634. [[CrossRef](#)]
26. Kwan, J.J.; Borden, M.A. Lipid monolayer collapse and microbubble stability. *Adv. Colloid Interface Sci.* **2012**, *183–184*, 82–99. [[CrossRef](#)]
27. Fokong, S.; Theek, B.; Wu, Z.; Koczera, P.; Appold, L.; Jorge, S.; Resch-Genger, U.; Van Zandvoort, M.; Storm, G.; Kiessling, F.; et al. Image-guided, targeted and triggered drug delivery to tumors using polymer-based microbubbles. *J. Control. Release* **2012**, *163*, 75–81. [[CrossRef](#)]
28. Skorb, E.V.; Möhwald, H. “smart” Surface Capsules for Delivery Devices. *Adv. Mater. Interfaces* **2014**, *1*, 1400237. [[CrossRef](#)]
29. Korolev, I.; Aliev, T.A.; Orlova, T.; Ulasevich, S.A.; Nosonovsky, M.; Skorb, E.V. When Bubbles Are Not Spherical: Artificial Intelligence Analysis of Ultrasonic Cavitation Bubbles in Solutions of Varying Concentrations. *J. Phys. Chem. B* **2022**, *126*, 3161–3169. [[CrossRef](#)]
30. Segers, T.; de Jong, N.; Versluis, M. Uniform scattering and attenuation of acoustically sorted ultrasound contrast agents: Modeling and experiments. *J. Acoust. Soc. Am.* **2016**, *140*, 2506–2517. [[CrossRef](#)]
31. Borden, M.A.; Longo, M.L. Dissolution behavior of lipid monolayer-coated, air-filled microbubbles: Effect of lipid hydrophobic chain length. *Langmuir* **2002**, *18*, 9225–9233. [[CrossRef](#)]
32. Grishenkov, D.; Kari, L.; Brodin, L.Å.; Brismar, T.B.; Paradossi, G. In vitro contrast-enhanced ultrasound measurements of capillary microcirculation: Comparison between polymer- and phospholipid-shelled microbubbles. *Ultrasonics* **2011**, *51*, 40–48. [[CrossRef](#)] [[PubMed](#)]
33. Chitnis, P.V.; Koppolu, S.; Mamou, L.; Chlon, C.; Ketterling, J.A. Influence of Shell Properties on High-Frequency Ultrasound Imaging and Drug. *IEEE Trans. Ultrason. Ferroelectr. Freq. Control* **2013**, *60*, 53–64. [[CrossRef](#)] [[PubMed](#)]
34. Liu, Z.; Chen, X. Simple bioconjugate chemistry serves great clinical advances: Albumin as a versatile platform for diagnosis and precision therapy. *Chem. Soc. Rev.* **2016**, *45*, 1432–1456. [[CrossRef](#)] [[PubMed](#)]
35. Rabbani, G.; Ahn, S.N. Structure, enzymatic activities, glycation and therapeutic potential of human serum albumin: A natural cargo. *Int. J. Biol. Macromol.* **2019**, *123*, 979–990. [[CrossRef](#)] [[PubMed](#)]
36. Zhu, G.; Lynn, G.M.; Jacobson, O.; Chen, K.; Liu, Y.; Zhang, H.; Ma, Y.; Zhang, F.; Tian, R.; Ni, Q.; et al. Albumin/vaccine nanocomplexes that assemble in vivo for combination cancer immunotherapy. *Nat. Commun.* **2017**, *8*, 1954. [[CrossRef](#)] [[PubMed](#)]
37. Sudlow, G.; Birkett, D.J.; Wade, D.N. The characterization of two specific drug binding sites on human serum albumin. *Mol. Pharmacol.* **1975**, *11*, 824–832. [[PubMed](#)]
38. Sudlow, G.; Birkett, D.J.; Wade, D.N. Further characterization of specific drug binding sites on human serum albumin. *Mol. Pharmacol.* **1976**, *12*, 1052–1061.
39. Zhu, L.; Yang, F.; Chen, L.; Meehan, E.J.; Huang, M. A new drug binding subsite on human serum albumin and drug-drug interaction studied by X-ray crystallography. *J. Struct. Biol.* **2008**, *162*, 40–49. [[CrossRef](#)]
40. Curry, S.; Brick, P.; Franks, N.P. Fatty acid binding to human serum albumin: New insights from crystallographic studies. *Biochim. Biophys. Acta-Mol. Cell Biol. Lipids* **1999**, *1441*, 131–140. [[CrossRef](#)]
41. Kratz, F. Albumin as a drug carrier: Design of prodrugs, drug conjugates and nanoparticles. *J. Control. Release* **2008**, *132*, 171–183. [[CrossRef](#)]
42. Keller, M.W.; Feinstein, S.B.; Watson, D.D. Successful left ventricular opacification following peripheral venous injection of sonicated contrast agent: An experimental evaluation. *Am. Heart J.* **1987**, *114*, 570–575. [[CrossRef](#)]
43. Keller, M.W.; Segal, S.S.; Kaul, S.; Duling, B. The behavior of sonicated albumin microbubbles within the microcirculation: A basis for their use during myocardial contrast echocardiography. *Circ. Res.* **1989**, *65*, 458–467. [[CrossRef](#)] [[PubMed](#)]
44. Keller, M.W.; Glasheen, W.; Kaul, S. Albunex: A Safe and Effective Commercially Produced Agent for Myocardial Contrast Echocardiography. *J. Am. Soc. Echocardiogr.* **1989**, *2*, 48–52. [[CrossRef](#)]

45. Ward, M.; Wu, J.; Chiu, J.F. Experimental study of the effects of optison[®] concentration on sonoporation in vitro. *Ultrasound Med. Biol.* **2000**, *26*, 1169–1175. [[CrossRef](#)]
46. Wei, K.; Mulvagh, S.L.; Carson, L.; Davidoff, R.; Gabriel, R.; Grimm, R.A.; Wilson, S.; Fane, L.; Herzog, C.A.; Zoghbi, W.A.; et al. The Safety of Definity and Optison for Ultrasound Image Enhancement: A Retrospective Analysis of 78,383 Administered Contrast Doses. *J. Am. Soc. Echocardiogr.* **2008**, *21*, 1202–1206. [[CrossRef](#)]
47. Hashiya, N.; Aoki, M.; Tachibana, K.; Taniyama, Y.; Yamasaki, K.; Hiraoka, K.; Makino, H.; Yasufumi, K.; Ogihara, T.; Morishita, R. Local delivery of E2F decoy oligodeoxynucleotides using ultrasound with microbubble agent (Optison) inhibits intimal hyperplasia after balloon injury in rat carotid artery model. *Biochem. Biophys. Res. Commun.* **2004**, *317*, 508–514. [[CrossRef](#)]
48. Li, T.; Tachibana, K.; Kuroki, M.; Kuroki, M. Gene Transfer with Echo—Enhanced Contrast Agents: Comparison between Albunex, Optison, and Levovist in Mice—Initial Results. *Radiology* **2003**, *229*, 423–428. [[CrossRef](#)]
49. Chumakova, O.V.; Liopo, A.V.; Mark Evers, B.; Esenaliev, R.O. Effect of 5-fluorouracil, optison and ultrasound on MCF-7 cell viability. *Ultrasound Med. Biol.* **2006**, *32*, 751–758. [[CrossRef](#)]
50. Sontum, P.C. Physicochemical Characteristics of Sonazoid[™], A New Contrast Agent for Ultrasound Imaging. *Ultrasound Med. Biol.* **2008**, *34*, 824–833. [[CrossRef](#)]
51. Schneider, M. Sono Vue, a new ultrasound contrast agent. *Eur. Radiol.* **1999**, *9*, 347–348. [[CrossRef](#)]
52. Greis, C. Technology overview: SonoVue (Bracco, Milan). *Eur. Radiol. Suppl.* **2004**, *14*, 11–15. [[CrossRef](#)]
53. Porter, T.R.; Iversen, P.L.; Li, S.; Xie, F. Interaction of diagnostic ultrasound with synthetic oligonucleotide-labeled perfluorocarbon-exposed sonicated dextrose albumin microbubbles. *J. Ultrasound Med.* **1996**, *15*, 577–584. [[CrossRef](#)] [[PubMed](#)]
54. Liao, A.H.; Wu, S.Y.; Wang, H.E.; Weng, C.H.; Wu, M.F.; Li, P.C. Evaluation of 18F-labeled targeted perfluorocarbon-filled albumin microbubbles as a probe for microUS and microPET in tumor-bearing mice. *Ultrasonics* **2013**, *53*, 320–327. [[CrossRef](#)] [[PubMed](#)]
55. Florinas, S.; Nam, H.Y.; Kim, S.W. Enhanced siRNA delivery using a combination of an Arginine-grafted bioreducible polymer, ultrasound, and microbubbles in cancer cells. *Mol. Pharm.* **2013**, *10*, 2021–2030. [[CrossRef](#)] [[PubMed](#)]
56. Chong, W.K.; Papadopoulou, V.; Dayton, P.A. Imaging with ultrasound contrast agents: Current status and future. *Abdom. Radiol.* **2018**, *43*, 762–772. [[CrossRef](#)] [[PubMed](#)]
57. Willmann, J.K.; Bonomo, L.; Testa, A.C.; Rinaldi, P.; Rindi, G.; Valluru, K.S.; Petrone, G.; Martini, M.; Lutz, A.M.; Gambhir, S.S. Ultrasound molecular imaging with BR55 in patients with breast & ovarian lesions: First-in-human results. *J. Clin. Oncol.* **2017**, *35*, 2133–2140. [[CrossRef](#)]
58. Smeenge, M.; Tranquart, F.; Mannaerts, C.K.; de Reijke, T.M.; van de Vijver, M.J.; Laguna, M.P.; Pochon, S.; de la Rosette, J.J.M.C.H.; Wijkstra, H. First-in-human ultrasound molecular imaging with a VEGFR2-specific ultrasound molecular contrast agent (BR55) in prostate cancer a safety and feasibility pilot study. *Investig. Radiol.* **2017**, *52*, 419–427. [[CrossRef](#)]
59. Köse, G.; Darguzyte, M.; Kiessling, F. Molecular ultrasound imaging. *Nanomaterials* **2020**, *10*, 1935. [[CrossRef](#)]
60. Manohar, S.; Dantuma, M. Current and future trends in photoacoustic breast imaging. *Photoacoustics* **2019**, *16*, 100134. [[CrossRef](#)]
61. Premarket Approval (PMA). Imagio Breast Imaging System. Available online: <https://www.accessdata.fda.gov/scripts/cdrh/cfdocs/cfpma/pma.cfm?id=P200003> (accessed on 1 April 2022).
62. Ando, Y.; Tabata, H.; Sanchez, M.; Cagna, A.; Koyama, D.; Krafft, M.P. Microbubbles with a Self-Assembled Poloxamer Shell and a Fluorocarbon Inner Gas. *Langmuir* **2016**, *32*, 12461–12467. [[CrossRef](#)]
63. Justeau, C.; Vela-Gonzalez, A.V.; Jourdan, A.; Riess, J.G.; Krafft, M.P. Adsorption of Cerium Salts and Cerium Oxide Nanoparticles on Microbubbles Can Be Induced by a Fluorocarbon Gas. *ACS Sustain. Chem. Eng.* **2018**, *6*, 11450–11456. [[CrossRef](#)]
64. Mendoza-Ortega, E.E.; Dubois, M.; Krafft, M.P. Fluorocarbon Gas Exposure Induces Disaggregation of Nanodiamond Clusters and Enhanced Adsorption, Enabling Medical Microbubble Formation. *ACS Appl. Nano Mater.* **2020**, *3*, 8897–8905. [[CrossRef](#)]
65. Lindner, J.R. Microbubbles in medical imaging: Current applications and future directions. *Nat. Rev. Drug Discov.* **2004**, *3*, 527–532. [[CrossRef](#)]
66. Upadhyay, A.; Dalvi, S.V. Microbubble Formulations: Synthesis, Stability, Modeling and Biomedical Applications. *Ultrasound Med. Biol.* **2019**, *45*, 301–343. [[CrossRef](#)]
67. Ma, X.; Bussonniere, A.; Liu, Q. A facile sonochemical synthesis of shell-stabilized reactive microbubbles using surface-thiolated bovine serum albumin with the Traut's reagent. *Ultrason. Sonochem.* **2017**, *36*, 454–465. [[CrossRef](#)] [[PubMed](#)]
68. Narihira, K.; Watanabe, A.; Sheng, H.; Endo, H.; Feril, L.B.; Irie, Y.; Ogawa, K.; Moosavi-Nejad, S.; Kondo, S.; Kikuta, T.; et al. Enhanced cell killing and apoptosis of oral squamous cell carcinoma cells with ultrasound in combination with cetuximab coated albumin microbubbles. *J. Drug Target.* **2018**, *26*, 278–288. [[CrossRef](#)] [[PubMed](#)]
69. Lindner, J.R.; Coggins, M.P.; Kaul, S.; Klivanov, A.L.; Brandenburger, G.H.; Ley, K. Microbubble Persistence in the Microcirculation During Ischemia/Reperfusion and Inflammation Is Caused by Integrin- and Complement-Mediated Adherence to Activated Leukocytes. *Circulation* **2000**, *101*, 668–675. [[CrossRef](#)]
70. Wang, Q.; Xue, C.; Zhao, H.; Qin, Y.; Zhang, X.; Li, Y. The fabrication of protein microbubbles with diverse gas core and the novel exploration on the role of interface introduction in protein crystallization. *Colloids Surf. A Physicochem. Eng. Asp.* **2020**, *589*, 124471. [[CrossRef](#)]
71. Wang, Y.H.; Chen, S.P.; Liao, A.H.; Yang, Y.C.; Lee, C.R.; Wu, C.H.; Wu, P.C.; Liu, T.M.; Wang, C.R.C.; Li, P.C. Synergistic delivery of gold nanorods using multifunctional microbubbles for enhanced plasmonic photothermal therapy. *Sci. Rep.* **2014**, *4*, 5685. [[CrossRef](#)]

72. Villanueva, F.S.; Jankowski, R.J.; Manaugh, C.; Wagner, W.R. Albumin microbubble adherence to human coronary endothelium: Implications for assessment of endothelial function using myocardial contrast echocardiography. *J. Am. Coll. Cardiol.* **1997**, *30*, 689–693. [[CrossRef](#)]
73. Upadhyay, A.; Dalvi, S.V. Synthesis, characterization and stability of BSA-encapsulated microbubbles. *RSC Adv.* **2016**, *6*, 15016–15026. [[CrossRef](#)]
74. Upadhyay, A.; Dalvi, S.V.; Gupta, G.; Khanna, N. Effect of PEGylation on performance of protein microbubbles and its comparison with lipid microbubbles. *Mater. Sci. Eng. C* **2017**, *71*, 425–430. [[CrossRef](#)] [[PubMed](#)]
75. Rovers, T.A.M.; Sala, G.; van der Linden, E.; Meinders, M.B.J. Effect of Temperature and Pressure on the Stability of Protein Microbubbles. *ACS Appl. Mater. Interfaces* **2016**, *8*, 333–340. [[CrossRef](#)] [[PubMed](#)]
76. Rovers, T.A.M.; Sala, G.; van der Linden, E.; Meinders, M.B.J. Disintegration of protein microbubbles in presence of acid and surfactants: A multi-step process. *Soft Matter* **2015**, *11*, 6403–6411. [[CrossRef](#)]
77. Rovers, T.A.M.; Sala, G.; van der Linden, E.; Meinders, M.B.J. Temperature is key to yield and stability of BSA stabilized microbubbles. *Food Hydrocoll.* **2016**, *52*, 106–115. [[CrossRef](#)]
78. Borrelli, M.J.; O'Brien, W.D.; Bernock, L.J.; Williams, H.R.; Hamilton, E.; Wu, J.; Oelze, M.L.; Culp, W.C. Production of uniformly sized serum albumin and dextrose microbubbles. *Ultrason. Sonochem.* **2012**, *19*, 198–208. [[CrossRef](#)]
79. Khan, A.H.; Surwase, S.; Jiang, X.; Edirisinghe, M.; Dalvi, S.V. Enhancing in Vitro Stability of Albumin Microbubbles Produced Using Microfluidic T-Junction Device. *Langmuir* **2022**, *38*, 5052–5062. [[CrossRef](#)]
80. Ji, J.; Ji, S.-Y.; He, X.; Ling, W.-P. Preparation of ultrasound microbubbles crosslinked to albumin nanoparticles packaged with tissue-type plasminogen activator gene plasmid and method of in vivo transfection. *J. Exp. Pharmacol.* **2011**, *3*, 35–41. [[CrossRef](#)]
81. Du, A.J.; Zhao, X.; Li, B.; Mou, Y.; Wang, Y. DNA-loaded microbubbles with crosslinked bovine serum albumin shells for ultrasound-promoted gene delivery and transfection. *Colloids Surf. B Biointerfaces* **2017**, *161*, 279–287. [[CrossRef](#)]
82. Liou, Y.R.; Wang, Y.H.; Lee, C.Y.; Li, P.C. Buoyancy-activated cell sorting using targeted biotinylated albumin microbubbles. *PLoS ONE* **2015**, *10*, e0125036. [[CrossRef](#)]
83. Liu, X.; Gong, P.; Song, P.; Xie, F.; Miller, A.L.; Chen, S.; Lu, L. Rapid conjugation of nanoparticles, proteins and siRNAs to microbubbles by strain-promoted click chemistry for ultrasound imaging and drug delivery. *Polym. Chem.* **2019**, *10*, 705–717. [[CrossRef](#)]
84. Liu, X.; Gong, P.; Song, P.; Xie, F.; Miller, A.L.; Chen, S.; Lu, L. Fast functionalization of ultrasound microbubbles using strain promoted click chemistry. *Biomater. Sci.* **2018**, *6*, 623–632. [[CrossRef](#)] [[PubMed](#)]
85. Suslick, K.S. Sonochemistry. *Science* **1990**, *247*, 1439–1445. [[CrossRef](#)] [[PubMed](#)]
86. Melino, S.; Zhou, M.; Tortora, M.; Paci, M.; Cavalieri, F.; Ashokkumar, M. Molecular properties of lysozyme-microbubbles: Towards the protein and nucleic acid delivery. *Amino Acids* **2012**, *43*, 885–896. [[CrossRef](#)]
87. Mahalingam, S.; Raimi-Abraham, B.T.; Craig, D.Q.M.; Edirisinghe, M. Formation of protein and protein-gold nanoparticle stabilized microbubbles by pressurized gyration. *Langmuir* **2015**, *31*, 659–666. [[CrossRef](#)]
88. Liao, A.H.; Hung, C.R.; Lin, C.F.; Lin, Y.C.; Chen, H.K. Treatment effects of lysozyme-shelled microbubbles and ultrasound in inflammatory skin disease. *Sci. Rep.* **2017**, *7*, 41325. [[CrossRef](#)]
89. Cavalieri, F.; Micheli, L.; Kaliappan, S.; Teo, B.M.; Zhou, M.; Palleschi, G.; Ashokkumar, M. Antimicrobial and biosensing ultrasound-responsive lysozyme-shelled microbubbles. *ACS Appl. Mater. Interfaces* **2013**, *5*, 464–471. [[CrossRef](#)]
90. Zhou, M.; Cavalieri, F.; Ashokkumar, M. Tailoring the properties of ultrasonically synthesised microbubbles. *Soft Matter* **2011**, *7*, 623–630. [[CrossRef](#)]
91. Zhou, M.; Leong, T.S.H.; Melino, S.; Cavalieri, F.; Kentish, S.; Ashokkumar, M. Sonochemical synthesis of liquid-encapsulated lysozyme microspheres. *Ultrason. Sonochem.* **2010**, *17*, 333–337. [[CrossRef](#)]
92. Zhou, M.; Cavalieri, F.; Ashokkumar, M. Modification of the size distribution of lysozyme microbubbles using a post-sonication technique. *Instrum. Sci. Technol.* **2012**, *40*, 51–60. [[CrossRef](#)]
93. Vong, F.; Son, Y.; Bhuiyan, S.; Zhou, M.; Cavalieri, F.; Ashokkumar, M. A comparison of the physical properties of ultrasonically synthesized lysozyme- and BSA-shelled microbubbles. *Ultrason. Sonochem.* **2014**, *21*, 23–28. [[CrossRef](#)] [[PubMed](#)]
94. Tchienbou-Magaia, F.L.; Cox, P.W. Tribological study of suspensions of cysteine-rich protein stabilized microbubbles and subsequent triphasic A/O/W emulsions. *J. Texture Stud.* **2011**, *42*, 185–196. [[CrossRef](#)]
95. Chen, Z.; Pulsipher, K.W.; Chattaraj, R.; Hammer, D.A.; Sehgal, C.M.; Lee, D. Engineering the Echogenic Properties of Microfluidic Microbubbles Using Mixtures of Recombinant Protein and Amphiphilic Copolymers. *Langmuir* **2019**, *35*, 10079–10086. [[CrossRef](#)] [[PubMed](#)]
96. Chen, Z.; Chattaraj, R.; Pulsipher, K.W.; Karmacharya, M.B.; Hammer, D.A.; Lee, D.; Sehgal, C.M. Photoacoustic and Ultrasound Dual-Mode Imaging via Functionalization of Recombinant Protein-Stabilized Microbubbles with Methylene Blue. *ACS Appl. Bio Mater.* **2019**, *2*, 4020–4026. [[CrossRef](#)] [[PubMed](#)]
97. Grinstaff, M.W.; Suslick, K.S. Air-filled proteinaceous microbubbles: Synthesis of an echo-contrast agent. *Proc. Natl. Acad. Sci. USA* **1991**, *88*, 7708–7710. [[CrossRef](#)] [[PubMed](#)]
98. Suslick, K.S.; Grinstaff, M.W.; Kolbeck, K.J.; Wong, M. Characterization of sonochemically prepared proteinaceous microspheres. *Ultrason. Sonochem.* **1994**, *1*, 65–68. [[CrossRef](#)]
99. Kohno, M.; Mokudai, T.; Ozawa, T.; Niwano, Y. Free radical formation from sonolysis of water in the presence of different gases. *J. Clin. Biochem. Nutr.* **2011**, *49*, 96–101. [[CrossRef](#)]

100. Asada, K.; Kanematsu, S. Reactivity of Thiols with Superoxide Radicals. *Agric. Biol. Chem.* **1976**, *40*, 1891–1892. [[CrossRef](#)]
101. Avivi, S.; Gedanken, A. S–S Bonds Are not Required for the Sonochemical Formation of Proteinaceous Microspheres: The Case of Streptavidin. *Biochem. J.* **2002**, *366*, 705–707. [[CrossRef](#)]
102. Murayama, K.; Tomida, M. Heat-induced secondary structure and conformation change of bovine serum albumin investigated by Fourier transform infrared spectroscopy. *Biochemistry* **2004**, *43*, 11526–11532. [[CrossRef](#)]
103. Majorek, K.A.; Porebski, P.J.; Dayal, A.; Zimmerman, M.D.; Jablonska, K.; Stewart, A.J.; Chruszcz, M.; Minor, W. Structural and immunologic characterization of bovine, horse, and rabbit serum albumins. *Mol. Immunol.* **2012**, *52*, 174–182. [[CrossRef](#)] [[PubMed](#)]
104. Lee, L.; Cavalieri, F.; Ashokkumar, M. Exploring New Applications of Lysozyme-Shelled Microbubbles. *Langmuir* **2019**, *35*, 9997–10006. [[CrossRef](#)] [[PubMed](#)]
105. Reisner, S.A.; Ong, L.S.; Lichtenberg, G.S.; Amico, A.F.; Shapiro, J.R.; Allen, M.N.; Meltzer, R.S. Myocardial perfusion imaging by contrast echocardiography with use of intracoronary sonicated albumin in humans. *J. Am. Coll. Cardiol.* **1989**, *14*, 660–665. [[CrossRef](#)]
106. Porter, T.R.; Abdelmoneim, S.; Belcik, J.T.; McCulloch, M.L.; Mulvagh, S.L.; Olson, J.J.; Porcelli, C.; Tsutsui, J.M.; Wei, K. Guidelines for the cardiac sonographer in the performance of contrast echocardiography: A focused update from the American society of echocardiography. *J. Am. Soc. Echocardiogr.* **2014**, *27*, 797–810. [[CrossRef](#)] [[PubMed](#)]
107. Chen, S.; Wang, Z.; Zhou, Y.T.; Grayburn, P.A. Optimization of the size distribution and myocardial contrast effect of perfluorocarbon-filled albumin microbubbles by lyophilization under continuous negative pressure. *J. Am. Soc. Echocardiogr.* **2000**, *13*, 748–753. [[CrossRef](#)] [[PubMed](#)]
108. Lindner, J.R.; Song, J.; Christiansen, J.; Klibanov, A.L.; Xu, F.; Ley, K. Ultrasound assessment of inflammation and renal tissue injury with microbubbles targeted to P-selectin. *Circulation* **2001**, *104*, 2107–2112. [[CrossRef](#)] [[PubMed](#)]
109. Lentacker, I.; de Geest, B.G.; Vandenbroucke, R.E.; Peeters, L.; Demeester, J.; de Smedt, S.C.; Sanders, N.N. Ultrasound-responsive polymer-coated microbubbles that bind and protect DNA. *Langmuir* **2006**, *22*, 7273–7278. [[CrossRef](#)]
110. Anderson, D.R.; Tsutsui, J.M.; Xie, F.; Radio, S.J.; Porter, T.R. The role of complement in the adherence of microbubbles to dysfunctional arterial endothelium and atherosclerotic plaque. *Cardiovasc. Res.* **2007**, *73*, 597–606. [[CrossRef](#)]
111. Anderson, D.R.; Duryee, M.J.; Anchan, R.K.; Garvin, R.P.; Johnston, M.D.; Porter, T.R.; Thiele, G.M.; Klassen, L.W. Albumin-based microbubbles bind up-regulated scavenger receptors following vascular injury. *J. Biol. Chem.* **2010**, *285*, 40645–40653. [[CrossRef](#)] [[PubMed](#)]
112. Talu, E.; Hettiarachchi, K.; Zhao, S.; Powell, R.L.; Lee, A.P.; Longo, M.L.; Dayton, P.A. Tailoring the size distribution of ultrasound contrast agents: Possible method for improving sensitivity in molecular imaging. *Mol. Imaging* **2007**, *6*, 384–392. [[CrossRef](#)]
113. Pulsipher, K.W.; Hammer, D.A.; Lee, D.; Sehgal, C.M. Engineering Theranostic Microbubbles Using Microfluidics for Ultrasound Imaging and Therapy: A Review. *Ultrasound Med. Biol.* **2018**, *44*, 2441–2460. [[CrossRef](#)] [[PubMed](#)]
114. Seo, M.; Gorelikov, I.; Williams, R.; Matsuura, N. Microfluidic assembly of monodisperse, nanoparticle-incorporated perfluorocarbon microbubbles for medical imaging and therapy. *Langmuir* **2010**, *26*, 13855–13860. [[CrossRef](#)] [[PubMed](#)]
115. Mashaghi, S.; Abbaspourrad, A.; Weitz, D.A.; van Oijen, A.M. Droplet microfluidics: A tool for biology, chemistry and nanotechnology. *TrAC Trends Anal. Chem.* **2016**, *82*, 118–125. [[CrossRef](#)]
116. Dixon, A.J.; Dhanaliwala, A.H.; Chen, J.L.; Hossack, J.A. Enhanced Intracellular Delivery of a Model Drug Using Microbubbles Produced by a Microfluidic Device. *Ultrasound Med. Biol.* **2013**, *39*, 1267–1276. [[CrossRef](#)]
117. Huang, D.; Zhang, X.; Zhao, C.; Fu, X.; Zhang, W.; Kong, W.; Zhang, B.; Zhao, Y. Ultrasound-Responsive Microfluidic Microbubbles for Combination Tumor Treatment. *Adv. Ther.* **2021**, *4*, 1–11. [[CrossRef](#)]
118. Farook, U.; Stride, E.; Edirisinghe, M.J.; Moaleji, R. Microbubbling by co-axial electrohydrodynamic atomization. *Med. Biol. Eng. Comput.* **2007**, *45*, 781–789. [[CrossRef](#)]
119. Mahalingam, S.; Meinders, M.B.J.; Edirisinghe, M. Formation, stability, and mechanical properties of bovine serum albumin stabilized air bubbles produced using coaxial electrohydrodynamic atomization. *Langmuir* **2014**, *30*, 6694–6703. [[CrossRef](#)]
120. Yan, W.C.; Ong, X.J.; Pun, K.T.; Tan, D.Y.; Sharma, V.K.; Tong, Y.W.; Wang, C.H. Preparation of tPA-loaded microbubbles as potential theranostic agents: A novel one-step method via coaxial electrohydrodynamic atomization technique. *Chem. Eng. J.* **2017**, *307*, 168–180. [[CrossRef](#)]
121. Mahalingam, S.; Xu, Z.; Edirisinghe, M. Antibacterial Activity and Biosensing of PVA-Lysozyme Microbubbles Formed by Pressurized Gyration. *Langmuir* **2015**, *31*, 9771–9780. [[CrossRef](#)]
122. Kukizaki, M.; Goto, M. Spontaneous formation behavior of uniform-sized microbubbles from Shirasu porous glass (SPG) membranes in the absence of water-phase flow. *Colloids Surf. A Physicochem. Eng. Asp.* **2007**, *296*, 174–181. [[CrossRef](#)]
123. Jang, Y.; Jang, W.S.; Gao, C.; Shim, T.S.; Crocker, J.C.; Hammer, D.A.; Lee, D. Tuning the Mechanical Properties of Recombinant Protein-Stabilized Gas Bubbles Using Triblock Copolymers. *ACS Macro Lett.* **2016**, *5*, 371–376. [[CrossRef](#)] [[PubMed](#)]
124. Chen, J.L.; Dhanaliwala, A.H.; Dixon, A.J.; Klibanov, A.L.; Hossack, J.A. Synthesis and characterization of transiently stable albumin-coated microbubbles via a flow-focusing microfluidic device. *Ultrasound Med. Biol.* **2014**, *40*, 400–409. [[CrossRef](#)] [[PubMed](#)]
125. Angilè, F.E.; Vargo, K.B.; Sehgal, C.M.; Hammer, D.A.; Lee, D. Recombinant protein-stabilized monodisperse microbubbles with tunable size using a valve-based microfluidic device. *Langmuir* **2014**, *30*, 12610–12618. [[CrossRef](#)] [[PubMed](#)]

126. Dhanaliwala, A.H.; Dixon, A.J.; Lin, D.; Chen, J.L.; Klivanov, A.L.; Hossack, J.A. In vivo imaging of microfluidic-produced microbubbles. *Biomed. Microdevices* **2015**, *17*, 23. [[CrossRef](#)]
127. Dixon, A.J.; Rickel, J.M.R.; Shin, B.D.; Klivanov, A.L.; Hossack, J.A. In Vitro Sonothrombolysis Enhancement by Transiently Stable Microbubbles Produced by a Flow-Focusing Microfluidic Device. *Ann. Biomed. Eng.* **2018**, *46*, 222–232. [[CrossRef](#)]
128. Parhizkar, M.; Sofokleous, P.; Stride, E.; Edirisinghe, M. Novel preparation of controlled porosity particle/fibre loaded scaffolds using a hybrid micro-fluidic and electrohydrodynamic technique. *Biofabrication* **2014**, *6*, 45010. [[CrossRef](#)]
129. Jiang, X.; Zhang, Y.; Edirisinghe, M.; Parhizkar, M. Combining microfluidic devices with coarse capillaries to reduce the size of monodisperse microbubbles. *RSC Adv.* **2016**, *6*, 63568–63577. [[CrossRef](#)]
130. Ojha, T.; Pathak, V.; Drude, N.; Weiler, M.; Rommel, D.; Rütten, S.; Geinitz, B.; Van Steenberg, M.J.; Storm, G.; Kiessling, F.; et al. Shelf-life evaluation and lyophilization of PBCA-based polymeric microbubbles. *Pharmaceutics* **2019**, *11*, 433. [[CrossRef](#)]
131. Miller, M.W. Gene transfection and drug delivery. *Ultrasound Med. Biol.* **2000**, *26*, 59–62. [[CrossRef](#)]
132. Shchukin, D.G.; Möhwald, H. Sonochemical nanosynthesis at the engineered interface of a cavitation microbubble. *Phys. Chem. Chem. Phys.* **2006**, *8*, 3496–3506. [[CrossRef](#)]
133. Cavalieri, F.; Ashokkumar, M.; Grieser, F.; Caruso, F. Ultrasonic synthesis of stable, functional lysozyme microbubbles. *Langmuir* **2008**, *24*, 10078–10083. [[CrossRef](#)] [[PubMed](#)]
134. Cavalieri, F.; Micheli, L.; Zhou, M.; Tortora, M.; Palleschi, G.; Ashokkumar, M. Electrochemical investigation of the interaction between lysozyme-shelled microbubbles and vitamin C. *Anal. Bioanal. Chem.* **2013**, *405*, 5531–5538. [[CrossRef](#)] [[PubMed](#)]
135. Cavalieri, F.; Zhou, M.; Ashokkumar, M.; Caruso, F. One-pot ultrasonic synthesis of multifunctional microbubbles and microcapsules using synthetic thiolated macromolecules. *Chem. Commun.* **2011**, *47*, 4096–4098. [[CrossRef](#)] [[PubMed](#)]
136. Chen, S.; Shohet, R.V.; Bekeredjian, R.; Frenkel, P.; Grayburn, P.A. Optimization of ultrasound parameters for cardiac gene delivery of adenoviral or plasmid deoxyribonucleic acid by ultrasound-targeted microbubble destruction. *J. Am. Coll. Cardiol.* **2003**, *42*, 301–308. [[CrossRef](#)]
137. Yoon, Y.I.; Pang, X.; Jung, S.; Zhang, G.; Kong, M.; Liu, G.; Chen, X. Smart gold nanoparticle-stabilized ultrasound microbubbles as cancer theranostics. *J. Mater. Chem. B* **2018**, *6*, 3235–3239. [[CrossRef](#)]
138. Barmin, R.A.; Rudakovskaya, P.G.; Chernyshev, V.S.; Guslyakova, O.I.; Sindeeva, O.A.; Prikhozhenko, E.S.; Bratashov, D.N.; Abdurashitov, A.S.; Maksimova, E.A.; Demina, P.A.; et al. Impact of fluorescent dyes on the physicochemical parameters of microbubbles stabilized by albumin-dye complex. *Colloids Surf. A Physicochem. Eng. Asp.* **2022**, *647*, 129095. [[CrossRef](#)]
139. Gorce, J.M.; Arditi, M.; Schneider, M. Influence of bubble size distribution on the echogenicity of ultrasound contrast agents: A study of sonovue(TM). *Investig. Radiol.* **2000**, *35*, 661–671. [[CrossRef](#)]
140. Newsome, I.G.; Kierski, T.M.; Dayton, P.A. Assessment of the Superharmonic Response of Microbubble Contrast Agents for Acoustic Angiography as a Function of Microbubble Parameters. *Ultrasound Med. Biol.* **2019**, *45*, 2515–2524. [[CrossRef](#)]
141. Park, J.I.; Jagadeesan, D.; Williams, R.; Oakden, W.; Chung, S.; Stanis, G.J.; Kumacheva, E. Microbubbles loaded with nanoparticles: A route to multiple imaging modalities. *ACS Nano* **2010**, *4*, 6579–6586. [[CrossRef](#)]
142. Gazzera, L.; Milani, R.; Pirrie, L.; Schmutz, M.; Blanck, C.; Resnati, G.; Metrangolo, P.; Krafft, M.P. Design of Highly Stable Echogenic Microbubbles through Controlled Assembly of Their Hydrophobin Shell. *Angew. Chem. Int. Ed.* **2016**, *55*, 10263–10267. [[CrossRef](#)]
143. Lukáč, R.; Kauerová, Z.; Mašek, J.; Bartheldyová, E.; Kulich, P.; Koudelka, Š.; Korvasová, Z.; Plocková, J.; Papoušek, F.; Kolář, F.; et al. Preparation of metalchelating microbubbles and study on their site-specific interaction with rGFP-HisTag as a model protein. *Langmuir* **2011**, *27*, 4829–4837. [[CrossRef](#)] [[PubMed](#)]
144. Abenojar, E.C.; Bederman, I.; de Leon, A.C.; Zhu, J.; Hadley, J.; Kolios, M.C.; Exner, A.A. Theoretical and experimental gas volume quantification of micro-and nanobubble ultrasound contrast agents. *Pharmaceutics* **2020**, *12*, 208. [[CrossRef](#)] [[PubMed](#)]
145. Wang, Y.-H.; Liao, A.-H.; Chen, J.-H.; Chris Wang, C.-R.; Li, P.-C. Photoacoustic/ultrasound dual-modality contrast agent and its application to thermotherapy. *J. Biomed. Opt.* **2012**, *17*, 045001. [[CrossRef](#)] [[PubMed](#)]
146. Guo, G.; Tu, J.; Guo, X.; Huang, P.; Wu, J.; Zhang, D. Characterization of mechanical properties of hybrid contrast agents by combining atomic force microscopy with acoustic/optic assessments. *J. Biomech.* **2016**, *49*, 319–325. [[CrossRef](#)] [[PubMed](#)]
147. Caudwell, J.A.; Tinkler, J.M.; Johnson, B.R.G.; McDowall, K.J.; Alsulaimani, F.; Tiede, C.; Tomlinson, D.C.; Freear, S.; Turnbull, W.B.; Evans, S.D.; et al. Protein-conjugated microbubbles for the selective targeting of *S. aureus* biofilms. *Biofilm* **2022**, *4*, 100074. [[CrossRef](#)]
148. Hosny, N.A.; Mohamedi, G.; Rademeyer, P.; Owen, J.; Wu, Y.; Tang, M.X.; Eckersley, R.J.; Stride, E.; Kuimova, M.K. Mapping microbubble viscosity using fluorescence lifetime imaging of molecular rotors. *Proc. Natl. Acad. Sci. USA* **2013**, *110*, 9225–9230. [[CrossRef](#)]
149. Park, B.; Yoon, S.; Choi, Y.; Jang, J.; Park, S.; Choi, J. Stability of engineered micro or nanobubbles for biomedical applications. *Pharmaceutics* **2020**, *12*, 1089. [[CrossRef](#)]
150. Wang, Y.; Xie, X.; Wang, X.; Ku, G.; Gill, K.L.; O'Neal, D.P.; Stoica, G.; Wang, L.V. Photoacoustic tomography of a nanoshell contrast agent in the in vivo rat brain. *Nano Lett.* **2004**, *4*, 1689–1692. [[CrossRef](#)]
151. Lu, W.; Huang, Q.; Ku, G.; Wen, X.; Zhou, M.; Guzatov, D.; Brecht, P.; Su, R.; Oraevsky, A.; Wang, L.V.; et al. Photoacoustic imaging of living mouse brain vasculature using hollow gold nanospheres. *Biomaterials* **2010**, *31*, 2617–2626. [[CrossRef](#)]
152. Hannah, A.; Luke, G.; Wilson, K.; Homan, K.; Emelianov, S. Indocyanine green-loaded photoacoustic nanodroplets: Dual contrast nanoconstructs for enhanced photoacoustic and ultrasound imaging. *ACS Nano* **2014**, *8*, 250–259. [[CrossRef](#)]

153. Dumani, D.S.; Sun, I.C.; Emelianov, S.Y. Ultrasound-guided immunofunctional photoacoustic imaging for diagnosis of lymph node metastases. *Nanoscale* **2019**, *11*, 11649–11659. [[CrossRef](#)] [[PubMed](#)]
154. Paproski, R.J.; Forbrich, A.; Huynh, E.; Chen, J.; Lewis, J.D.; Zheng, G.; Zemp, R.J. Porphyrin Nanodroplets: Sub-micrometer Ultrasound and Photoacoustic Contrast Imaging Agents. *Small* **2016**, *12*, 371–380. [[CrossRef](#)] [[PubMed](#)]
155. De Groot, P.G.; Reinders, J.H.; Sixma, J.J. Perturbation of human endothelial cells by thrombin or PMA changes the reactivity of their extracellular matrix towards platelets. *J. Cell Biol.* **1987**, *104*, 697–704. [[CrossRef](#)] [[PubMed](#)]
156. Mulder, A.B.; Hegge-Paping, K.S.M.; Magielse, C.P.E.; Blom, N.R.; Smit, J.W.; van der Meer, J.; Halie, M.R.; Bom, V.J.J. Tumor necrosis factor α -induced endothelial tissue factor is located on the cell surface rather than in the subendothelial matrix. *Blood* **1994**, *84*, 1559–1566. [[CrossRef](#)]
157. Bevilacqua, M.P.; Pober, J.S.; Wheeler, M.E.; Cotran, R.S.; Gimbrone, M.A.J. Interleukin 1 acts on cultured human vascular endothelium to increase the adhesion of polymorphonuclear leukocytes, monocytes, and related leukocyte cell lines. *J. Clin. Investig.* **1985**, *76*, 2003–2011. [[CrossRef](#)]
158. Zwaginga, J. Activation of Endothelial Cells Induces Platelet Thrombus Formation on their Matrix. *Atherosclerosis* **1989**, *10*, 49–61.
159. Schnitzer, J.E.; Carley, W.W.; Palade, G.E. Specific albumin binding to microvascular endothelium in culture. *Am. J. Physiol.-Heart Circ. Physiol.* **1988**, *254*, H425–H437. [[CrossRef](#)]
160. Schnitzer, J.E.; Oh, P. Antibodies to SPARC inhibit albumin binding to SPARC, gp60, and microvascular endothelium. *Am. J. Physiol.-Heart Circ. Physiol.* **1992**, *263*, H1872–H1879. [[CrossRef](#)]
161. Gimbrone, M.A. Vascular endothelium: An integrator of pathophysiological stimuli in atherosclerosis. *Am. J. Cardiol.* **1995**, *75*, 67B–70B. [[CrossRef](#)]
162. Meredith, I.T.; Anderson, T.J.; Uehata, A.; Yeung, A.C.; Selwyn, A.P.; Ganz, P. Role of endothelium in ischemic coronary syndromes. *Am. J. Cardiol.* **1993**, *72*, 27C–31C. [[CrossRef](#)]
163. Anderson, T.J.; Gerhard, M.D.; Meredith, I.T.; Charbonneau, F.; Delagrang, D.; Creager, M.A.; Selwyn, A.P.; Ganz, P. Systemic nature of endothelial dysfunction in atherosclerosis. *Am. J. Cardiol.* **1995**, *75*, 71B–74B. [[CrossRef](#)]
164. Cybulsky, M.I.; Gimbrone, M.A. Endothelial expression of a mononuclear leukocyte adhesion molecule during atherogenesis. *Science* **1991**, *251*, 788–791. [[CrossRef](#)] [[PubMed](#)]
165. Ross, R. The pathogenesis of atherosclerosis: A perspective for the 1990s. *Nature* **1993**, *362*, 801–809. [[CrossRef](#)] [[PubMed](#)]
166. Cheng, Y.; Cheng, H.; Jiang, C.; Qiu, X.; Wang, K.; Huan, W.; Yuan, A.; Wu, J.; Hu, Y. Perfluorocarbon nanoparticles enhance reactive oxygen levels and tumour growth inhibition in photodynamic therapy. *Nat. Commun.* **2015**, *6*, 8785. [[CrossRef](#)] [[PubMed](#)]
167. You, Y.; Liang, X.; Yin, T.; Chen, M.; Qiu, C.; Gao, C.; Wang, X.; Mao, Y.; Qu, E.; Dai, Z.; et al. Porphyrin-grafted lipid microbubbles for the enhanced efficacy of photodynamic therapy in prostate cancer through ultrasound-controlled in situ accumulation. *Theranostics* **2018**, *8*, 1665–1677. [[CrossRef](#)]
168. Brilkina, A.A.; Dubasova, L.V.; Sergeeva, E.A.; Pospelov, A.J.; Shilyagina, N.Y.; Shakhova, N.M.; Balalaeva, I.V. Photobiological properties of phthalocyanine photosensitizers Photosens, Holosens and Phthalosens: A comparative in vitro analysis. *J. Photochem. Photobiol. B Biol.* **2019**, *191*, 128–134. [[CrossRef](#)]
169. Alzeibak, R.; Mishchenko, T.A.; Shilyagina, N.Y.; Balalaeva, I.V.; Vedunova, M.V.; Krysko, D. V Targeting immunogenic cancer cell death by photodynamic therapy: Past, present and future. *J. Immunother. Cancer* **2021**, *9*, e001926. [[CrossRef](#)]
170. Cavalieri, F.; Zhou, M.; Ashokkumar, M. The Design of Multifunctional Microbubbles for Ultrasound Image-Guided Cancer Therapy. *Curr. Top. Med. Chem.* **2010**, *10*, 1198–1210. [[CrossRef](#)]
171. Cavalieri, F.; Zhou, M.; Tortora, M.; Lucilla, B.; Ashokkumar, M. Methods of Preparation of Multifunctional Microbubbles and their In Vitro/In Vivo Assessment of Stability, Functional and Structural Properties. *Curr. Pharm. Des.* **2012**, *18*, 2135–2151. [[CrossRef](#)]
172. Tsutsui, J.M.; Xie, F.; Porter, R.T. The use of microbubbles to target drug delivery. *Cardiovasc. Ultrasound* **2004**, *2*, 23. [[CrossRef](#)]
173. Bao, S.; Thrall, B.D.; Miller, D.L. Transfection of a reporter plasmid into cultured cells by sonoporation in vitro. *Ultrasound Med. Biol.* **1997**, *23*, 953–959. [[CrossRef](#)]
174. Shohet, R.V.; Chen, S.; Zhou, Y.T.; Wang, Z.; Meidell, R.S.; Unger, R.H.; Grayburn, P.A. Echocardiographic destruction of albumin microbubbles directs gene delivery to the myocardium. *Circulation* **2000**, *101*, 2554–2556. [[CrossRef](#)] [[PubMed](#)]
175. Bekerdedjian, R.; Chen, S.; Frenkel, P.A.; Grayburn, P.A.; Shohet, R.V. Ultrasound-targeted microbubble destruction can repeatedly direct highly specific plasmid expression to the heart. *Circulation* **2003**, *108*, 1022–1026. [[CrossRef](#)] [[PubMed](#)]
176. Taniyama, Y.; Tachibana, K.; Hiraoka, K.; Namba, T.; Yamasaki, K.; Hashiya, N.; Aoki, M.; Ogihara, T.; Yasufumi, K.; Morishita, R. Local delivery of plasmid DNA into rat carotid artery using ultrasound. *Circulation* **2002**, *105*, 1233–1239. [[CrossRef](#)] [[PubMed](#)]
177. Frenkel, P.A.; Chen, S.; Thai, T.; Shohet, R.V.; Grayburn, P.A. DNA-loaded albumin microbubbles enhance ultrasound-mediated transfection in vitro. *Ultrasound Med. Biol.* **2002**, *28*, 817–822. [[CrossRef](#)]
178. Fleming, A.; Allison, V.D. Observations on a Bacteriolytic Substance (“Lysozyme”) Found in Secretions and Tissues. *Br. J. Exp. Pathol.* **1922**, *3*, 252–260.
179. Varahan, S.; Iyer, V.S.; Moore, W.T.; Hancock, L.E. Eep confers lysozyme resistance to enterococcus faecalis via the activation of the extracytoplasmic function sigma factor SigV. *J. Bacteriol.* **2013**, *195*, 3125–3134. [[CrossRef](#)]
180. Samaranayake, Y.H.; Cheung, B.P.K.; Parahitiyawa, N.; Seneviratne, C.J.; Yau, J.Y.Y.; Yeung, K.W.S.; Samaranayake, L.P. Synergistic activity of lysozyme and antifungal agents against *Candida albicans* biofilms on denture acrylic surfaces. *Arch. Oral Biol.* **2009**, *54*, 115–126. [[CrossRef](#)]

181. Sheikov, N.; McDannold, N.; Vykhodtseva, N.; Jolesz, F.; Hynynen, K. Cellular mechanisms of the blood-brain barrier opening induced by ultrasound in presence of microbubbles. *Ultrasound Med. Biol.* **2004**, *30*, 979–989. [[CrossRef](#)]
182. Lammers, T.; Koczera, P.; Fokong, S.; Gremse, F.; Ehling, J.; Vogt, M.; Pich, A.; Storm, G.; Van Zandvoort, M.; Kiessling, F. Theranostic USPIO-loaded microbubbles for mediating and monitoring blood-brain barrier permeation. *Adv. Funct. Mater.* **2015**, *25*, 36–43. [[CrossRef](#)]
183. Wu, S.K.; Tsai, C.L.; Huang, Y.; Hynynen, K. Focused ultrasound and microbubbles-mediated drug delivery to brain tumor. *Pharmaceutics* **2021**, *13*, 15. [[CrossRef](#)]
184. Kost, J.; Mitragotri, S.; Gabbay, R.A.; Pishko, M.; Langer, R. Transdermal monitoring of glucose and other analytes using ultrasound. *Nat. Med.* **2000**, *6*, 347–350. [[CrossRef](#)] [[PubMed](#)]
185. Azagury, A.; Khoury, L.; Enden, G.; Kost, J. Ultrasound mediated transdermal drug delivery. *Adv. Drug Deliv. Rev.* **2014**, *72*, 127–143. [[CrossRef](#)] [[PubMed](#)]
186. Schnaider, L.; Shimonov, L.; Kreiser, T.; Zaguri, D.; Bychenko, D.; Brickner, I.; Kolusheva, S.; Lichtenstein, A.; Kost, J.; Gazit, E. Ultrashort Cell-Penetrating Peptides for Enhanced Sonophoresis-Mediated Transdermal Transport. *ACS Appl. Bio Mater.* **2020**, *3*, 8395–8401. [[CrossRef](#)] [[PubMed](#)]